

COO-3069-327
OSP-73622
Conf-450654--1

HADRON AND PHOTON PRODUCTION OF J PARTICLES
AND
THE ORIGIN OF J PARTICLES

Samuel C. C. Ting

Department of Physics and
Laboratory for Nuclear Science
Massachusetts Institute of Technology

RECEIVED BY TIC AUG 6 1975

A Rapporteur's Summary at the International
Conference on High Energy Physics
Palermo, Sicily. June, 1975

MASTER

DISTRIBUTION OF THIS DOCUMENT UNLIMITED

DISCLAIMER

This report was prepared as an account of work sponsored by an agency of the United States Government. Neither the United States Government nor any agency Thereof, nor any of their employees, makes any warranty, express or implied, or assumes any legal liability or responsibility for the accuracy, completeness, or usefulness of any information, apparatus, product, or process disclosed, or represents that its use would not infringe privately owned rights. Reference herein to any specific commercial product, process, or service by trade name, trademark, manufacturer, or otherwise does not necessarily constitute or imply its endorsement, recommendation, or favoring by the United States Government or any agency thereof. The views and opinions of authors expressed herein do not necessarily state or reflect those of the United States Government or any agency thereof.

DISCLAIMER

Portions of this document may be illegible in electronic image products. Images are produced from the best available original document.

NOTICE

This report was prepared as an account of work sponsored by the United States Government. Neither the United States nor the United States Energy Research and Development Administration, nor any of their employees, nor any of their contractors, subcontractors, or their employees, makes any warranty, express or implied, or assumes any legal liability or responsibility for the accuracy, completeness or usefulness of any information, apparatus, product or process disclosed, or represents that its use would not infringe privately owned rights.

COPY - 750654 -- 1

INTRODUCTION

There have been many theoretical speculations ¹⁾ on the existence of long lived neutral particles with a mass larger than $10 \text{ GeV}/c^2$ which play the role in weak interactions that photons play in electromagnetic interactions. There is, however, no theoretical justification, and no predictions exist, for long lived particles in the mass region $1-10 \text{ GeV}/c^2$.

Even though there is no strong theoretical justification for the existence of long lived particles at low masses, there is no experimental indication that they should not exist. Until last year no high sensitivity experiment had been done in this mass region.

There are calculations based on parton models on the production of an e^+e^- continuum from pp interactions. ²⁾ An early experiment at the AGS ³⁾ studied the continuum of $\mu^+\mu^-$ from $p+\text{Uranium} \rightarrow \mu^+\mu^- + X$. This experiment gives approximately the size of $\mu^+\mu^-$ yield. In the last ten years there have been many experiments ⁴⁾ at Brookhaven, at CERN I.S.R., at Fermi Lab, etc. to study the inclusive $e(\mu)$ production $P+P \rightarrow e(\mu) + X$. Again, these experiments gave no indication of a long lived particle.

My report will consist of three chapters:

1. The Discovery of the J Particle
2. The Production of the J Particle by Hadrons and Photons
3. The Origin of the J Particle

Chapter One: Discovery of the J Particle

The discovery of the J Particle ^{5,6,7)} in proton-proton collisions by the MIT-BNL group at Brookhaven National Laboratory follows a decade of experiments associated with e^+e^- pair productions from hadron interactions at high energies. One learns three kinds of physics from the reaction

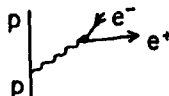
$$h + p \rightarrow e^+e^- + X.$$

- (i) Using a 7.5 GeV bremsstrahlung photon beam one can compare the e^+e^- yield with predictions of QED at large momentum transfer or small distances, $<10^{-14} \text{ cm}$. ⁸⁾
- (ii) One can study the e^+e^- decay of photon-like particles with spin 1 and negative parity and charge conjugation, such as the ρ , ⁹⁾ ϕ , ¹⁰⁾ ω , ¹¹⁾ and ρ , ¹²⁾ and measure the coupling strengths between photons and massive photon-like particles. ¹³⁾ One can also study the production mechanisms of these photon-like particles produced by photons.
- (iii) Search for additional particles which decay to e^+e^- from $pp \rightarrow e^+e^- + X$ or $pp \rightarrow \mu^+\mu^- + X$.

1.1 Design Considerations: To perform a high sensitivity experiment, detecting narrow width particles over a wide mass region, we make the

following four observations:

- (i) Since the e^+e^- comes from photon decays, the yield of e^+e^- is lower than hadron pairs ($\pi^+\pi^-$, K^+K^- , pp , K^+p , etc.) by a factor



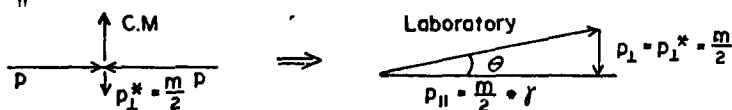
$$\frac{\alpha^2}{m^4} F^2(m^2) \approx 10^{-6}$$

The factor α^2 comes from the virtual photon decay, m^{-4} is the photon propagator and $F(m^2)$ the form factor of the target proton, where m is the invariant mass of the e^+e^- pair.

- (ii) Because of (i) one must design a detector which can stand a high flux of hadrons to obtain a sufficient yield of e^+e^- pairs.
 (iii) The detector must be able to reject hadron pairs by a factor $\sim 10^6 - 10^8$.
 (iv) In choosing the best kinematic region to detect the decay of new particles, one notes that at high energies, inclusive production of ρ , π and ω from p - p interactions can all be described in the c.m. system by a dependence of the form

$$\frac{d^3\sigma}{dp_{\parallel}^* dp_{\perp}^{*2}} = \frac{ae^{-bp_{\perp}^*}}{E^*}, \text{ independent of } p_{\parallel}^*,$$

where p_{\parallel}^* , p_{\perp}^* and E^* have their usual meaning.



Thus the maximum yield will occur when the particle is produced at rest in the center of mass. If we look at the 90° decay of the e^+e^- pair, we note that they emerge at an angle $\theta = \arctan\left(\frac{1}{\gamma}\right) = 14.6^\circ$ in the lab system for an incident proton energy of 28.5 GeV, independent of the mass of the decaying particle.

1.2 Experimental Set-up: Figure 1 shows the plan and side views of the spectrometer and detectors. Bending is done vertically to decouple angle (θ) and momentum. The field of the magnets in their final location was measured with a three dimensional Hall probe at a total of 10^5 points. C_B , C_O and C_e are gas threshold Cerenkov counters. C_B is filled with isobutane at 1 atm., C_O is filled with hydrogen at 1 atm. and C_e is filled with hydrogen at 0.8 atm. A_O , A, B and C are proportional wire chambers with 2 mm spacing and a total of 4,000 wires on each arm. Behind chambers A and B are situated two planes of hodoscopes, 8×8 , for improved timing resolution.

Behind the C chamber there are two orthogonal banks of lead glass counters of three radiation lengths each, the first containing twelve elements, the second thirteen, followed by one horizontal bank of lead lucite shower counters, seven in number, each ten radiation lengths thick,

to further reject hadrons from electrons and improve track identification.

The following are the unique features of this experiment:

- (i) To obtain a rejection against hadrons of 10^8 or better, the two gas Cerenkov counters in each arm, C_0 and C_e (Fig. 2a, b) are filled with hydrogen and made with thin mylar windows to reduce knock-on and scintillation effects. The counters are painted black inside and are decoupled by the strong magnetic fields of M_1 and M_2 , so that knock-on electrons produced in C_0 do not enter C_e and only electrons along the beam trajectory will emit Cerenkov light which is focussed onto the photomultiplier tube. Special high gain, high efficiency phototubes of the type RCA C31000M were used so that the counters C_0 and C_e can be operated at 100% efficiency with very low voltage. The counter C_0 collects an average of 9 photoelectrons. To ensure the voltage was set on a single electron and not on e^+e^- pairs from π^0 's, which would give ~ 18 photoelectrons, the counter C_0 was filled with He and the location of the single photoelectron peak was found (Fig. 2C).
- (ii) To be able to handle a high intensity of 2×10^{12} protons per pulse with consequent single arm rates of ~ 20 MHz, there are eleven planes of proportional wires ($2xA_0$, $3xA$, $3xB$, and $3xC$) rotated 20° with respect to each other as shown in Fig. 3a to reduce multitrack ambiguities. To ensure the chambers have a 100% uniform efficiency at low voltage (Fig. 3b) and a long live time in the highly radioactive environment, a special Argon-Methylal mixture at 2°C was used.
- (iii) To reduce multiple scattering and photon conversion, the material in the beam is reduced to a minimum. The front and rear windows of C_0 are $125 \mu\text{m}$ thick respectively, both mirrors of C_0 and C_e are made of 3 mm black lucite and hodoscopes are 1.6 mm thick.
The thickness of one piece of Beryllium target is 1.8 mm and the nine pieces are each separated by 7.5 cm so that the particles produced in one piece and accepted by the spectrometer do not pass through the next piece.
- (iv) To reduce photon and neutron contamination the location of all the hodoscopes and lead glass counters are such that they do not see the target directly. To further shield the detectors from soft neutrons, 10,000 lbs. of Borax soap was placed on top of C_0 between M_1 and M_2 and around the front part of C_e behind M_2 .
- (v) To improve the rejection against $\pi^0 \rightarrow \gamma e^+e^-$, a very directional Cerenkov counter C_B was placed close to the target and below a specially constructed magnet M_0 (Fig. 4a). This counter is painted black inside and is sensitive to electrons of 10 MeV/c and pions above 2.7 GeV/c. The coincidence between C_B and C_0 ,

C_e the shower counters and the hodoscopes indicates the detection of an e^+e^- pair from the process $\pi^0 \rightarrow \gamma e^+e^-$, and such events are rejected. A typical plot of the relative timing of this coincidence is shown in Fig. 4b. Conversely, one can trigger on C_B and provide a pure electron beam to calibrate C_0 , C_e and the shower counters. This is a redundant check in setting the voltage of the C_0 counters, since the coincidence between C_0 and C_B will ensure that the counter is efficient for a single electron and not a zero degree pair.

- (vi) The spectrometer has a very large mass acceptance of $2 \text{ GeV}/c^2$ and enables us to study the mass region $1.5 - 5.5 \text{ GeV}/c^2$ in three overlapping settings. For a point target the acceptance in θ is $\pm 1^\circ$, in ϕ it is $\pm 2^\circ$ and in momentum it varies from $0.6 \times p_0$ to $1.8 \times p_0$ (where p_0 is the principal axis momentum), all in the lab. system.

The following table summarizes the important properties of the MIT-BNL experiment:

Unique Features

1. Can stand incident flux of 2×10^{12} protons/pulse.
or 20 MC single rates.
 $\sigma_B \Rightarrow 10^{-36} \text{ cm}^2$.
2. Sort out 8 tracks per arm.
3. Rejection $\frac{e^-e^+}{h^-h^+} \ll 10^{-8}$.
4. Mass resolution $\pm 5 \text{ MeV}$.
5. Mass acceptance 2 BeV.

1.3 First Results: The first data from August 1974 are shown in Fig. 5a. There is a clear, sharp enhancement at a mass of $3.1 \text{ GeV}/c^2$.

To ensure that the observed peak is a real particle, from August to November experimental checks were made on the data. I list six examples:

- (i) The magnet currents were decreased by 10%, the peak remained fixed at $3.1 \text{ GeV}/c^2$ (see Fig. 5a).
- (ii) To check second order effects on the target, the target thickness was increased by a factor of two. The yield increased by a factor of two, not by four.
- (iii) To check for pile up in the lead glass and shower counters, different runs were made with different voltage settings on the counters. No effect was observed on the yield of J.

- (iv) To insure that the peak is not due to scattering from the sides of the magnets, cuts were made in the data to reduce the effective aperture. No significant reduction in the J yield was found.
- (v) To check the read-out system of the chambers and the triggering system of the hodoscopes, runs were made with a few planes of chambers deleted and with sections of the hodoscopes omitted from the trigger. No effect was observed on the J yield.
- (vi) Runs with different beam intensity were made and the yield did not change.

These and many other checks convinced us that we have observed a real massive particle $J \rightarrow e^+e^-$.

Partial analysis of the width of the J particle shown in Fig. 5b indicates it has a width smaller than $5 \text{ MeV}/c^2$.

If we assume a production mechanism for J to be

$$\frac{d^3 \sigma}{dp_{\perp}^{*2} dp_{\parallel}^*} = \frac{e^{-6p_{\perp}^*}}{E^*}, \text{ independent of } p_{\parallel}^*$$

and an isotropic decay in the rest system of the J, we obtain a $J \rightarrow e^+e^-$ yield of $10^{-34} \text{ cm}^2/\text{nucleon}$ at 28.5 GeV.

Fig. 6 shows the yield of e^+e^- in the region 3.2 to 4.0 GeV/c^2 , normalized to Fig. 5a. The acceptance in this region is a smooth function and varies at most by a factor of two. The observed events are consistent with purely random coincidences. To a level of 1% of the J yield, with a confidence level of 95%, no heavier J particles were found. We note that this upper limit is independent of any production mechanism of the J, we obtain an upper limit of $10^{-36} \text{ cm}^2/\text{nucleon}$ for the production of heavier J's with a 95% confidence level.

Fig. 7 shows the very preliminary results measured on a single piece of target in the fall of 1974 for inclusive e^- yield. Shown in Fig. 7a and b are the target reconstruction and shower pulse height information, showing that the observed signal is real electrons with little hadron background. No detailed analysis has yet been made. The data shown in Fig. 7c as function of converter thickness indicate a ratio $\frac{e^-}{\pi^-} \approx 10^{-4}$ at $p_{\perp} \approx 1\text{-}2 \text{ GeV}$.

Chapter Two: Photoproduction of J by Photons and Hadrons

Since the discovery of the J particle some very important experiments have been carried out at Cornell, at SLAC, at Fermilab, and at the ISR. These experiments show that the J particle is not the intermediate vector Boson. But it is a hadron, and production of J by photons proceeds diffractively off complex nuclei like photoproduction of ρ^0 off nuclei. Production of J from Nucleon-Nucleon interaction increases by ~ 100 from $s=60 \text{ GeV}^2$ to $s=3000 \text{ GeV}^2$, similarly to the increase in yield of K mesons in this energy range. Let me describe a few of the most important experiments:

2.1 Production by photons:

2.1.1 The experimental setup at Cornell¹⁴⁾ (Fig. 8a) consisted of passing a collimated bremsstrahlung beam of 11.8 GeV endpoint energy through a 2.9 g/cm^2 beryllium target. The target was viewed by a pair of lead glass Cerenkov hodoscopes. The lead glass hodoscopes have an energy resolution of $\delta E/E \approx 12/\sqrt{E} \text{ GeV}$, rms, (Fig. 8b) and a position resolution of $\delta s = 0.5 \text{ cm}$, rms. They were located $\sim 150 \text{ cm}$ downstream from the target and separated vertically from the beam by $\sim 48 \text{ cm}$. A seven counter scintillation hodoscope was installed directly in front of each glass hodoscope.

An event trigger consisted of a coincidence between the two lead glass hodoscopes for which the energy in each was greater than $\sim 2.5 \text{ GeV}$ and the sum of their energies was greater than 7.0 GeV . Data were taken at an incident beam intensity of 2×10^{11} equivalent quanta/minute. A total of 3×10^{15} equivalent quanta were used.

Knowing the energy and position at the counter of each particle and assuming they came from the target, one constructs their momentum vectors. From these, the mass squared, m_x^2 , and the angle of production of the two particle system, θ_x are computed. One notes the bump at $m_x^2 \sim 9 \text{ GeV}^2$ (Fig. 9). Also shown are the contributions from Bethe-Heitler pairs and measured backgrounds.

The $t-t_{\min}$ distribution of the events in the mass squared range $7.5-11.0 \text{ GeV}^2$ are shown in Fig. 10. The solid line shown here was calculated from a production cross section of the form $A e^{1.2t}$ by folding in the detector acceptance and the decay distribution of a spin 1 meson. They obtain:

$$\begin{aligned} A &= 0.8 \pm 0.2 \text{ nb/GeV}^2 \\ b &= 1.2 \pm 0.3 \text{ GeV}^{-2} \end{aligned}$$

Gittelman and Silverman have pointed out the significance of the small value for the slope parameter, b. It may just reflect the fact that only a few partial waves are involved because of the low J momentum (in the center of the mass) or it may reflect a small interaction radius.

2.1.2 The second experiment¹⁵⁾ was carried out by Camerini, Prepost, Ritson and Collaborators from Wisconsin and SLAC. The experiment used the

SLAC 8 GeV and 20 GeV spectrometers instrumented to detect both electron and muon pairs from J decay. The spectrometers were set for 90° decay in the J rest system. A bremsstrahlung beam from a 5% radiator was incident on 30.3 cm H_2 or D_2 targets. The end point energy was 0.5 GeV or 1.0 GeV above J energy. The overall accuracy of beam intensity was monitored to 3%.

Electrons were identified by a threshold gas Cerenkov counter, a lead glass preradiator, and a lead-lucite shower counter. Muons were identified with an iron-scintillation counter range telescope. The single arm muon yields were typically 3-4% of the pion flux and a factor of 20-30 higher than the single arm electron yields.

The resolution of the detectors was approximately .15% in momentum and 0.3 mrad in production angle, giving an invariant mass resolution of 20 MeV (FWHM) at mass of 3 GeV. The mass acceptance of the system was 150 MeV (FWHM).

Assuming elastic J production, with a $(1 + \cos^2 \theta^*)$ J $\rightarrow e^-e^+$ decay and known branching ratio for J $\rightarrow e^-e^+$, the results are presented in the table below and Figures 11a and 11b. The errors indicated in the table are statistical only. The overall systematic error for the cross sections is estimated to be 15%. In order to compare cross sections as a function of energy, the t_{min} data have been extrapolated to $t=0$ by the correction factor $e^{-bt_{min}}$ with $b=2.9$ (GeV/c) $^{-2}$. The resultant J $t=0$ cross sections are shown as a function of photon energy in Figure 11a. Figure 11b shows the $k=19$ GeV, $E_0=20$ GeV data points as a function of t .

Summary Table

K (GeV)	(K = photon energy, E_0 = end point energy)		t' (GeV/c) 2	$d\sigma/dt(t)$ [nb/(GeV/c) 2]
	E_0 (GeV)	t_{min} (GeV/c) 2		
a. J from Deuterium Target				
21.0	21.5	0.069	0.0	14.6 ± 1.2
19.0	20.0	0.088	0.0	15.0 ± 1.0
19.0	19.5	0.088	0.0	12.0 ± 1.1
17.0	17.5	0.116	0.0	10.8 ± 1.0
16.0	16.5	0.135	0.0	8.2 ± 1.1
15.0	20.0	0.160	0.0	7.7 ± 1.5
15.0	16.0	0.160	0.0	5.9 ± 1.0
13.0	13.5	0.236	0.0	3.8 ± 0.8
19.0	20.0	0.088	0.20	8.2 ± 1.1
19.0	20.0	0.088	0.40	4.9 ± 0.7
b. J from Hydrogen Target				
19.0	19.5	0.088	0.0	10.8 ± 1.1
c. 3.7 from Deuterium Target				
21.0	21.5	0.164	0.0	4.3 ± 1.6

$$t' \equiv (t - t_{\min})$$

The main features of the results are as follows:

- (i) The D_2-H_2 cross section per nucleon ratio is

$$\frac{d\sigma/dt|_{D_2}}{d\sigma/dt|_{H_2}} = 1.12 \pm .16 \quad \text{At } E_0=20.0 \quad K=19.5 \text{ GeV}$$

indicating that J production from the proton and neutron is very similar.

- (ii) Several points taken with different bremsstrahlung end point energies indicate a possible 20-30% inelastic contribution. The measurement made at t_{\min} with $k=15$ GeV and $E_0=16$ GeV and $E_0=20$ GeV indicates that inclusive J production contributions to the cross section are small. Specifically, using the notation (k, E_0) , the cross section ratios were determined to be

$$\frac{d\sigma/dt(19,20)}{d\sigma/dt(19,19.5)} = 1.25 \pm 1.4 \quad \text{and}$$

$$\frac{d\sigma/dt(15,20)}{d\sigma/dt(15,16)} = 1.3 \pm .3$$

- (iii) The t distribution at $k=19$ GeV, $E_0=20$ GeV has a fitted slope parameter $b=2.9 \pm .3(\text{GeV}/c)^{-2}$ where b is defined by $d\sigma/dt \sim e^{bt}$.
- (iv) A small sample of data was taken with an incident electron beam. Subtracting the contribution from real and virtual photons, the direct electron production cross section for the J is determined to be $\leq 5\%$ of the photon production cross section.
- (v) 3.7p photoproduction has been observed at t_{\min} for $k=21$ GeV. The cross section ratio at t_{\min} is: $\frac{d\sigma/dt(J)}{d\sigma/dt(3700)} = 3.4 \pm 1.2$
- (vi) Assuming J dominance $\frac{d\sigma}{dt}\Big|_{t=0}(\gamma N \rightarrow JN) = \frac{\alpha}{4} \left(\frac{YJ^2}{4\pi}\right)^{-1} \frac{d\sigma}{dt}\Big|_{t=0}(JN \rightarrow JN)$

giving a value of $\frac{d\sigma}{dt}\Big|_{t=0}(JN \rightarrow JN) \approx 25 \mu\text{b}/(\text{GeV}/c)^2$

If in addition, the phase of forward J-N scattering amplitude is assumed to be pure imaginary, the optical theorem can be used to determine the J total cross section. This procedure yields

$$\sigma_{J,tot} \approx 0.8 \text{ mb}$$

2.1.3 Photoproduction of J at 100-200 BeV region:

A very beautiful and important experiment was done by the group of W. Lee, D. Yount, and T. O'Halloran, A. Wattenberg, J. Peoples and Collaborators from Columbia, Hawaii, Cornell, Illinois and Fermilab.¹⁶⁾ This was the first experiment to use a 100-200 BeV photon beam from a proton accelerator and shows that J particle is a hadron.

The photons are obtained from a 0-mrad neutral beam which is produced by the interactions of 300-GeV protons in a 30.5-cm Be target. The γ -to-n ratio is improved by a factor of roughly 200 above the γ -to-n ratio at production by passing the beam through 34 m of liquid D₂. The photon spectrum at the experimental target is shown in Fig. 12a.

The detector, which is shown in Fig. 12b, consists of a multiwire-proportional-chamber magnetic spectrometer and a particle identifier. The spectrometer magnet, M2, which has a field integral of 20 kG m, bends the trajectories of charged particles vertically.

The particle identifier consists of an electron (and photon) calorimeter, a hadron calorimeter, and a muon identifier. The electron calorimeter is made up of an upstream and a downstream shower-counter hodoscope. Each hodoscope is split into two identical halves which are separated horizontally from each other by 10 cm, in order to allow the beam and the copiously produced e^+e^- pairs to pass through.

The momentum resolution in the limit of a uniform field is calculated to be $\delta p/p = 0.02 [p \text{ in } (\text{GeV}/c)/100]$.

The raw mass spectrum for all events with momenta greater than 80 GeV/c is shown in Fig. 12c. The two principal features of these data which can be seen readily, are a preponderance of events at low mass, characteristic of muon-pair production by the Bethe-Heitler mechanism, and a peak at $3.1 \text{ GeV}/c^2$.

The measured cross section in the neutron experiment and the known ratio of photons to neutrons in the beam indicate <3 events in this experiment originated from neutrons in the beam.

The t distribution of the $J \rightarrow \mu^-\mu^+$ events is shown in Fig. 13. The curve shown in the figure is the calculated t distribution, corrected for acceptance and resolution, assuming $d\sigma(\gamma + \text{Be} \rightarrow J)/dt$ is proportional to $A^2 e^{40t} + Ae^{bt}$, where A is the atomic number of the Be nucleus. They conclude therefore, that the J is photoproduced diffractively on the Be nucleus. The simplest explanation for this behavior is that the J couples directly to the photon in the same way as do the ρ , ω , and ϕ . They found that the value of $1 < b < 4$ is quite consistent with the data. Their results can be summarized as:

- a. Based on 114 events $\sigma(\gamma + \text{Be} \rightarrow J + X) = 20 \pm 5 \text{ nb/nucleus}$
- b. Extrapolating the data to $t=0$, using vector dominance, assuming pure imaginary scattering, they obtain $\sigma(Jp) \approx 1 \text{ mb}$. This implies J is a hadron.
- c. They also observed 2 events of $3.7 \rightarrow \pi\pi J$ and $\gamma + \text{Pb} \rightarrow J + X$.

Summary of Photoproduction of J

1. J is a hadron	$\sigma_{JN} \approx 1 \text{ mb}$
2. $\gamma + A \rightarrow A + J$	diffractive production
3. E_0 (GeV)	$b \text{ GeV}^{-2}$
11.8	1.2 ± 0.3
20	$2.9 \pm .3$
80-200	1-4

4. Using the relation $\left. \frac{d\sigma}{dt} \right|_{\theta=0} = e^{bt_{MN}} \left. \frac{d\sigma}{dt} \right|_{t=0}$, $t_{MN} = \frac{mJ^4}{4K^2}$ we present the summary of $\left. \frac{d\sigma}{dt} \right|_{\theta=0}$ in Fig. 14. Also shown are the expected $\left. \frac{d\sigma}{dt} \right|_{\theta=0}$ increase with K. As seen, the forward cross section increases much faster than expected.

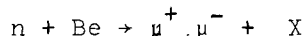
2.2 Hadron Production of J Particles

The data on hadron production of J, also show an increase in yield as function of energy. I list 3 experiments, one in each energy region as examples.

2.2.1 At BNL the MIT-BNL group measured the yield of J with a 20 BeV incident proton beam on Be target and found the J yield decreases by almost a factor of 10.

The preliminary P_{\perp}^2 dependence at 30 GeV is shown in Fig. 15. The data is consistent with $e^{-1.6P_{\perp}^2}$.

2.2.2 At Fermilab: the Columbia, Hawaii, Cornell, Illinois, Fermilab Collaboration¹⁷⁾ measured the reaction



The neutron experiment used the same detectors as their photon experiment but differed from the photon experiment in two respects. First, the 34 m of liquid deuterium was emptied and 3.8 cm of Pb was placed upstream in the neutral-beam line, thereby selectively attenuating the photons. The neutral beam was then predominantly neutrons. Secondly, a Be-Fe absorber was inserted behind the Be target to attenuate the hadrons and to reduce decay path of pions to 1.5 m. Fig. 16b shows the neutron energy spectrum. As seen, the photon contamination is small. The measured dimuon spectrum is shown in Fig. 16b. Both $\rho \rightarrow \mu^+ \mu^-$ and $J \rightarrow \mu^+ \mu^-$ are observed. Analysis of $\rho \rightarrow \mu^+ \mu^-$ data yield a $\frac{d\sigma}{dt} \propto e^{-6P_{\perp}^2}$ for $P_{\perp}^2 < 1$ GeV. Analysis of $J \rightarrow \mu^+ \mu^-$ data as function of P_{\perp}^2 is shown in Fig. 17. This data is consistent with $e^{-0.04 P_{\perp}^2}$ distribution. After correcting the acceptance they obtain:

$$\begin{aligned} \sigma(n+Be \rightarrow J+X) &= 3.6 \times 10^{-33} \text{ cm}^2/\text{nucleon}, |X| > 0.24 \\ &\stackrel{\mu^+\mu^-}{=} 1.7 \times 10^{-33} \text{ cm}^2/\text{nucleon}, |X| > 0.32 \end{aligned}$$

These cross sections are accurate to factor of 2, depending on the assumption of P_{\perp} dependence.

2.2.3 J production at I.S.R.:¹⁸⁾ The CERN - Columbia - Rockefeller-Saclay group performed an experiment at I.S.R. with a two arm spectrometer shown in Fig. 18.

Each spectrometer consisted of a system of wire spark chambers with magnetostrictive read-out and a magnet with a bending power of 3.4 kGm providing a momentum measurement with a standard deviation

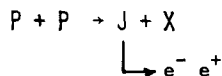
$$\Delta p/p = \sqrt{(0.025)^2 + (0.02p)^2} \quad (p \text{ in GeV}/c).$$

Electron identification was achieved by means of threshold gas Cerenkov counters and electromagnetic shower detectors. Counter C was filled with isobutane (C_4H_{10}) at atmospheric pressure. The corresponding pion momenta at threshold were 2.7 and 5.6 GeV/c respectively.

The electromagnetic shower detector in Arm 1 has an energy resolution of $\frac{\Delta E}{E} = 30\%$. The r.m.s. energy resolution of Arm 2 was measured to be $\Delta E/E = 0.017 + 0.064/\sqrt{E}$ (E in GeV). The detection efficiency for Arm 1 is $84 \pm 4\%$ and the hadron rejection factor is $> 3 \times 10^3$. The corresponding numbers in Arm 2 being $45 \pm 5\%$ and $> 2 \times 10^4$ respectively.

Each arm also contained three scintillation counter hodoscopes (H_1, H_2, H_3 , in Arm 1, and H'_1, H'_2, H'_3 in Arm 2). Hodoscope H_1 and H'_1 were equipped with pulse-height measuring electronics. To compute the acceptance they take a $\langle P_{\perp}^* \rangle = 0.67$ which is consistent with their data and an $e^{-3P_{\perp}^*}$ dependence. And, the decay angular distribution was taken to be isotropic in the rest system of the pair.

The table and graph below summarize all the data taken at various energies.

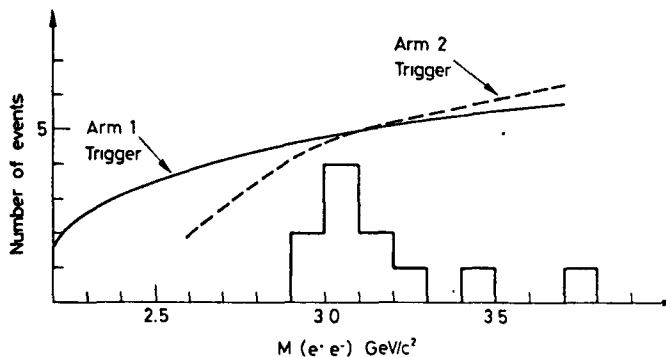


$$\frac{d\sigma}{dy} = (7.5 \pm 2.5) \times 10^{-33} \text{ cm}^2$$

$$\langle P_T \rangle^* = 0.67$$

$$d\sigma = (3.8 \pm 1.3) \times 10^{-32} \text{ cm}^2$$

\sqrt{S} GeV	30.6	44.8	52.7	62.4
running time (%)	16,	27,	50,	7
average $\sqrt{S} = 48$ GeV				



The cross section increases by 60% if one calculates the acceptance with $\langle P_{\perp}^* \rangle = 1.0$

The value of the cross section for J production at ISR energies is two orders of magnitude higher than the corresponding value quoted at BNL energies. A comparison with Fermilab measurement is more difficult since the experiments are done in disjoint regions of rapidity, but the cross sections appear to be of the same order of magnitude.

Chapter Three: The Origin of the J Particle

There have been hundreds of theoretical papers appearing in journals on the new particles.

The model of Glashow¹⁹⁾ views the J particle as a bound (Ortho) state of Charm (C) and Anti-Charm. In this model there would be a (Para) state $J \rightarrow \bar{p}p$ near 3.1 GeV. Furthermore, the charmed particle $C \rightarrow K\pi$ should be observed in the mass region 1.5 - 2.5 GeV.

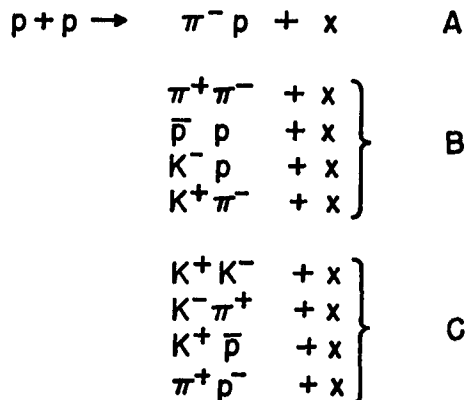
The model of Yang and Wu,¹⁹⁾ which views the J particle production from p p reaction to be via $p + p \rightarrow J \theta + X$ to conserve the possible additional quantum numbers of the J particle, would predict a long lived $\theta \rightarrow \pi^- p$ particle near the mass of 2 GeV.

Independent of theories, one can ask two important experimental questions.

How many other narrow resonances exist ?

Why the inclusive ratio $e/\pi \approx 10^{-4}$?

To answer these questions the MIT group has just completed a sytematic search of



in the pair mass region 1.2 - 5.0 BeV with a mass resolution of 5 MeV.

The expermental set up for this experiment is very similar to the original e^+e^- experiment. However since there are much more hadrons than electrons the random accidentals are more serious. To reduce the accidentals to minimum a new target system was put in. This consists of 5 pieces of 4 mm x 4 mm x 4 mm Be target separated from each other by six inches. The targets are supported by thin piano wires. This arrangement enables one to locate the point of intersection between the two trajectories.

Comparing it with the target location enables us to reduce the random accidentals (Fig.19a). To further reduce the accidentals additional scintillation counters were installed to tighten the two arm coincidence to 0.9 ns (Fig. 19b). Two high pressure (300 psi) Cerenkov counters were installed replacing the shower counters to identify K's. The counters C_e (Fig. 1) were filled with 1 atm isobutane to identify π 's. The Cerenkov counters set the mass acceptance to ~ 1 BeV. In this way all 9 combinations were measured simultaneously. To avoid systematic errors, 6 overlapping magnet settings were made for the measurement.

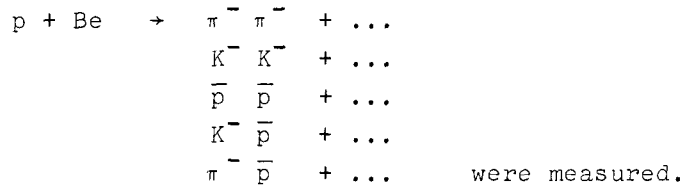
Figures 20-28 show the results of the 9 reactions. Without acceptance corrections the yield increases with mass due to an increase in acceptance and then decreases due to the decrease in production cross sections. As seen there are no sharp narrow resonances in any of the 9 reactions. There may be of course very wide "ordinary" resonances with widths of 300 MeV or more. A search for these depends on exact calculations of acceptance and has not yet been made. To obtain a feeling of the sensitivities of the measurements, we take the production of the 9 reactions to be the same as the assumed J production mechanisms. From this we obtain the following table:

SENSITIVITY (cm^2)
FOR NARROW RESONANCES

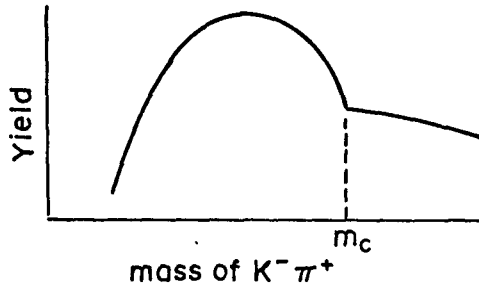
$h^+ X^- \backslash m$	2.25 GeV	3.1 GeV
$\pi^+ \pi^-$	8×10^{-33}	5×10^{-34}
$\pi^+ K^-$	1×10^{-33}	4×10^{-35}
$\pi^+ \bar{p}$	2×10^{-33}	4×10^{-35}
$K^+ \pi^-$	4×10^{-33}	8×10^{-35}
$K^+ K^-$	1×10^{-33}	5×10^{-35}
$K^+ \bar{p}$	2×10^{-33}	4×10^{-35}
$p \pi^-$	4×10^{-32}	4×10^{-33}
$p K^-$	7×10^{-33}	4×10^{-34}
$p \bar{p}$	—	4×10^{-34}

Whereas the spectra do not show any sharp resonance states the cross sections $\frac{d\sigma}{dm}$ vs m for groups A (π^-p), B ($\pi^+\pi^-, \bar{p}p, K^+\pi^-, K^-p$) and C ($K^+K^-, K^+p, \pi^+\bar{p}, K^-\pi^+$) do exhibit some simple degeneracies above the mass of J. The cross section for each group decreases with m as $\sim e^{-4m}$ and differ from each other by an order of magnitude.

To search for multibody final states additional reactions;



When one measures the two particle spectrum to search for multibody decays like $C \rightarrow K^-\pi^+\pi^-$, etc. one would expect a discontinuity in the $K^-\pi^+$ spectrum near the mass of C:



No such discontinuities were found.

The IHEP-CERN collaboration²⁰⁾ reported an experiment using a 40 GeV/c π^- Beam to study the exclusive reaction $\pi^- + p \rightarrow m\gamma + n$, $m=2,3,4$. The experiment used an H_2 target surrounded by a set of veto counters selecting neutral final states with γ -rays going in a forward cone. These γ -rays were detected in a 648-channel hodoscope spectrometer. During the running time 10^7 events were collected. 1/4 of the total statistics were analyzed corresponding to a sensitivity of $2.X 10^{-35} \text{cm}^2/\text{event}$.

As an illustration of the performance of the detection system and of the data treatment procedure, we show in Fig.29a results from a small part of the statistics, analyzed without invariant mass preselection: $n \rightarrow 2\gamma$, $\omega \rightarrow \pi^0\gamma$ and $f \rightarrow 2\pi^0$ are clearly seen. At higher masses the procedure for finding the showers works even better because of the more favourable topology and we expect $\Delta M/M = \pm 5\%$.

Fig. 29b shows results of the analysis for $M > 2.2$ GeV with various fits satisfied by the events. The general behavior is similar for all channels and there is no evident narrow structure in any of the invariant mass spectra. In the following table we give the 90% C.L. upper limits for the production cross section of a narrow width particle multiplied by its decay branching ratio in the mode considered, at the invariant mass values 3.1 and 3.7 GeV. The limits include corrections for the branching ratios $n \rightarrow 2\gamma / n \rightarrow \text{all} = 0.38$ and $X^0 \rightarrow 2\gamma / X^0 \rightarrow \text{all} = 0.025$, for the detection

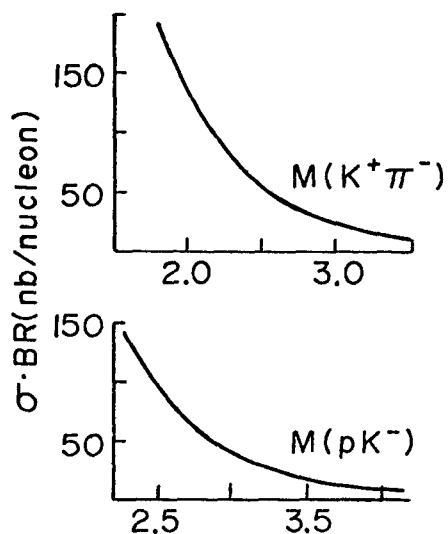
efficiency of the apparatus as well as for estimated losses of the shower recognition and of the kinematical analysis programs. Using the $J \rightarrow \pi^0 \gamma$ decay from DESY to be $< 2\%$ they obtain an upper limit on two body $\pi^- p \rightarrow J + n$ to be $< 2 \times 10^{-38} \text{ cm}^2$ which is 50 times less than the normal cross sections. The authors interpret this as strong support of $J \rightarrow C\bar{C}$ model.

TABLE

90% C.L. upper limits for the production cross section of a narrow width particle multiplied by the decay branching ratio in the mode considered, in units of 10^{-34} cm^2 . The estimated overall detection efficiency is taken into account.

Decay mode M, GeV	$\pi^0 \pi^0$	$\eta \eta$	$\pi^0 \gamma$	$\eta \gamma$	$X^0 \gamma$	$\gamma \gamma$
3.1	5	6	4	3	20	1.3
3.7	1.5	3	1.5	1	10	0.6

The experiment of the Fermilab, Northwestern, Rochester, SLAC Collaborators (private communication from T. Ferbec to S. Ting) measured $\pi\pi$, K^+K^- , $K^+\pi^-$, K^-p from $N+Be$ reactions at ~ 200 BeV. The result shown in the diagram below also does not exhibit sharp peaks.



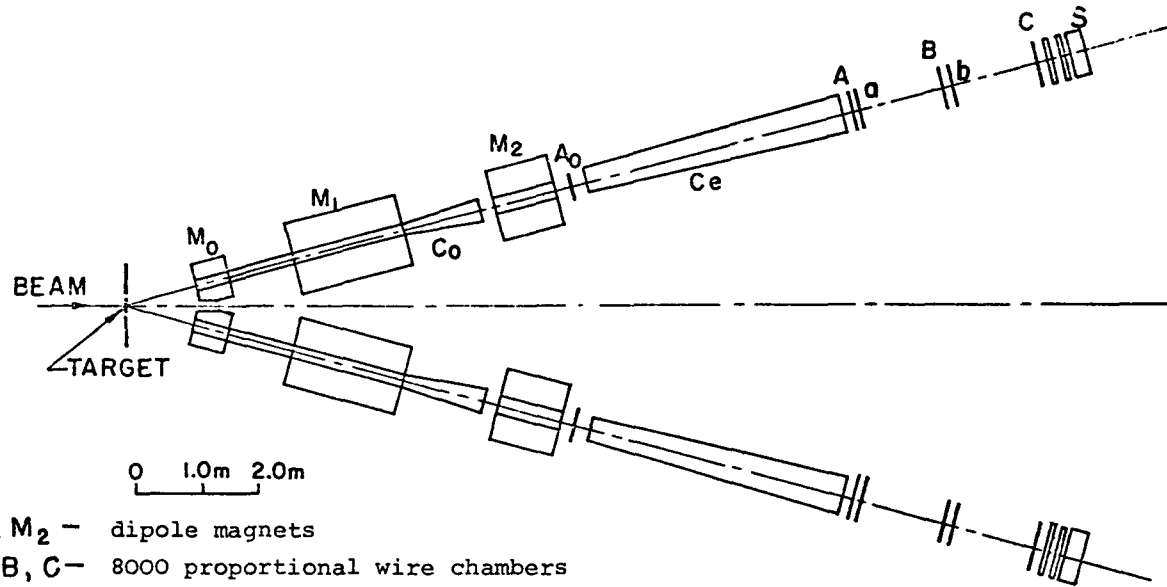
There are many other experiments at I.S.R., Fermilab etc. designed to find Charmed particles. So far no definite positive results have been reported.

Acknowledgement

I wish to thank Professor A. Zichichi for his hospitality during the conference. I am grateful for conversations with Drs. W.Y. Lee, L. Di Lella, B. Gittelman, T. O'Halloran, B. Pope, D. Ritson, A. Silverman M. Tannenbaum on their experiments. I am also grateful to Dr. J. Burger, Ms. S.C. Marks, Mr. Cyril Tourtellotte, Mr. W. Toki and Dr. S.L. Wu for their help in preparing this work.

REFERENCES

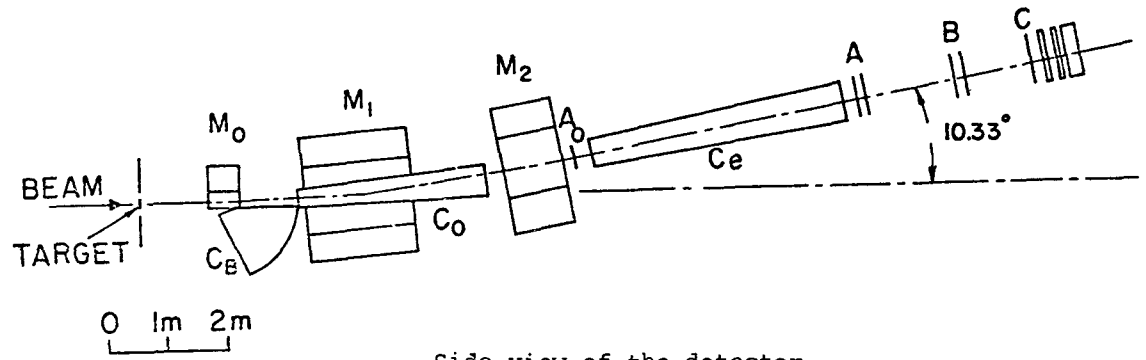
- 1) T.D. Lee, Phys. Rev. Lett. 26, 801 (1971);
S. Weinberg, Phys. Rev. Lett. 19, 1264 (1967); Phys. Rev. Lett. 27,
1688 (1971); Phys. Rev. Lett. D5, 1412 (1972) and Phys. Rev. D5, 1962
(1972);
A. Salam, in Elementary Particle Theory, edited by N. Svartholm
(Almqvist and Farlag, Stockholm, 1968).
- 2) S.D. Drell and T.M. Yan, Phys. Rev. Lett. 25, 316 (1970).
- 3) J.H. Christenson et al., Phys. Rev. Lett. 25, 1523 (1970).
- 4) R. Burns et al., Phys. Rev. Lett. 15, 830 (1965)
J.P. Boymond et al., Phys. Rev. Lett. 33, 112 (1974)
J.A. Appel et al., Phys. Rev. Lett. 33, 722 (1974)
F.W. Büsser et al., Phys. Rev. Lett. 53B (1974) 212
L.B. Leipuner et al., Phys. Rev. Lett. 34, 103 (1975).
- 5) J.J. Aubert et al., Phys. Rev. Lett. 33, 1404 (1974).
- 6) J.E. Augustin et al., Phys. Rev. Lett. 33, 1406 (1974).
- 7) C. Bacci et al., Phys. Rev. Lett. 33, 1408 (1974).
- 8) J.G. Asbury et al., Phys. Rev. Lett. 18, 65 (1967);
H. Alvensleben et al., Phys. Rev. Lett. 21, 1501 (1968).
- 9) J.G. Asbury et al., Phys. Rev. Lett. 19, 869 (1967).
- 10) U. Becker et al., Phys. Rev. Lett. 21, 1504 (1968).
- 11) H. Alvensleben et al., Phys. Rev. Lett. 25, 1373 (1970);
P. Biggs et al., Phys. Rev. Lett. 24, 1197 (1970).
- 12) G. Barbarino et al., Lett. al Nuovo Cimento 3, 693 (1972).
- 13) J.G. Asbury et al., Phys. Rev. Lett. 19, 865 (1967);
H. Alvensleben et al., Phys. Rev. Lett. 24, 786 (1970);
H. Alvensleben et al., Phys. Rev. Lett. 28, 66 (1972);
K. Gottfried, 1971 International Symposium on Electron/Photon
Interactions at High Energies, Cornell (1971); see references listed
therein.
- 14) B. Gittelman, K. Hanson, D. Larson, E. Loh, A. Silverman and G.
Theodosiou, Contribution to this conference and private communication
from Drs. Gittelman and Silverman to Ting.
- 15) U. Camerinin et al., contribution to this conference and private
communication.
- 16) B. Knapp et al., Phys. Rev. Lett. 34, 1040 (1975), and contribution
to this conference and private communication.
- 17) B. Knapp et al., Phys. Rev. Lett. 34, 1044 (1975), and contribution
to this conference and private communication.
- 18) F. Büsser et al., contribution to this conference and private
communication.
- 19) H.T Nieh, T.T. Wu, and C.N. Yang, Phys. Rev. Lett. 34, 49 (1975);
A. de Rujula and S.L. Glashow, Phys. Rev. Lett. 34, 46 (1975);
C.G. Callam, R.L. Kingsley, S.B. Treiman, F. Wilczek and A. Zee,
Phys. Rev. Lett. 34, 52 (1975); J.J. Sakurai, Phys. Rev. Lett. 34, 56
(1975).
- 20) Yu. D. Prokoshkin et al., contribution to this conference.



M_0, M_1, M_2 - dipole magnets
 A_0, A, B, C - 8000 proportional wire chambers
 a, b - 8x8 hodoscopes
 S - 3 banks of pb-glass
 shower counters
 C_B, C_0, C_e - gas cerenkov counters

Plan view of the detector

Fig. 1a



Side view of the detector

Fig. 1b

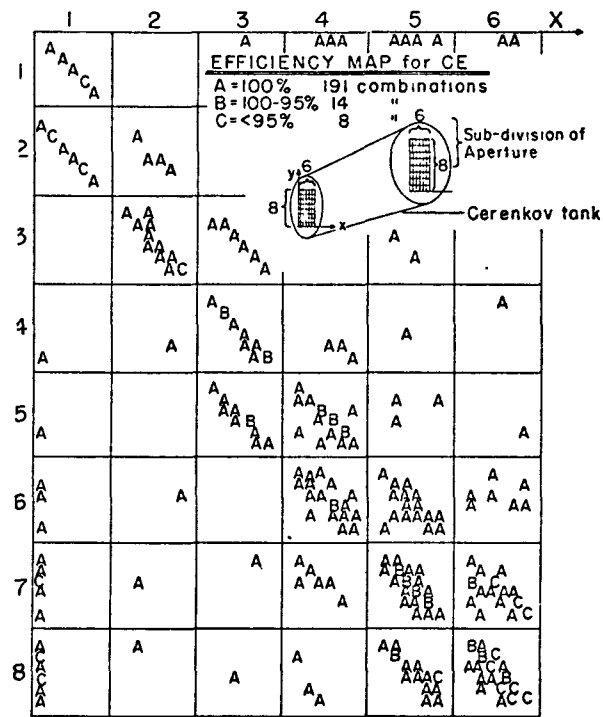
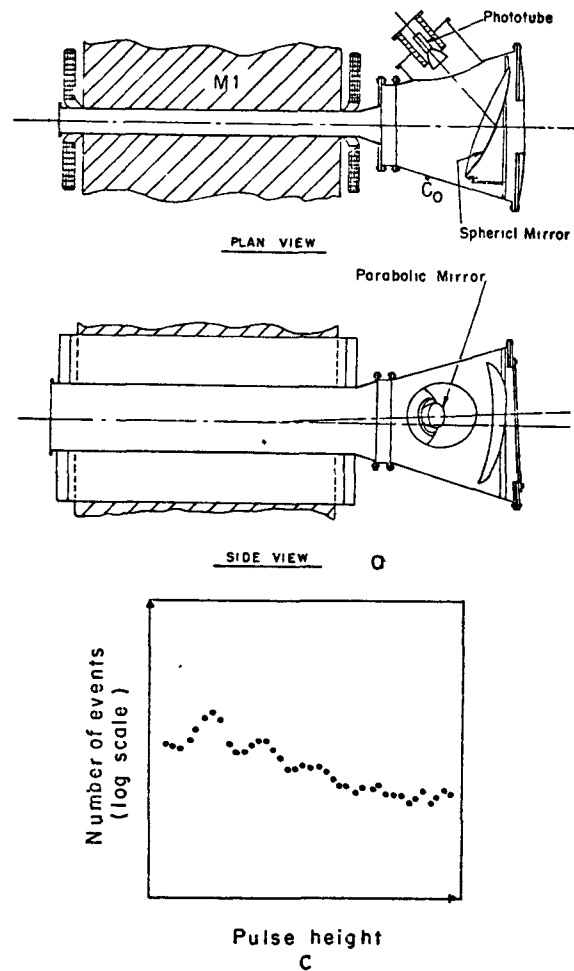
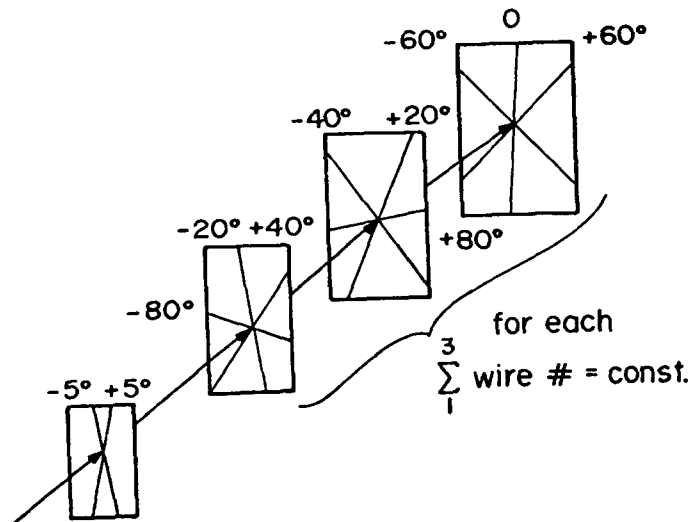


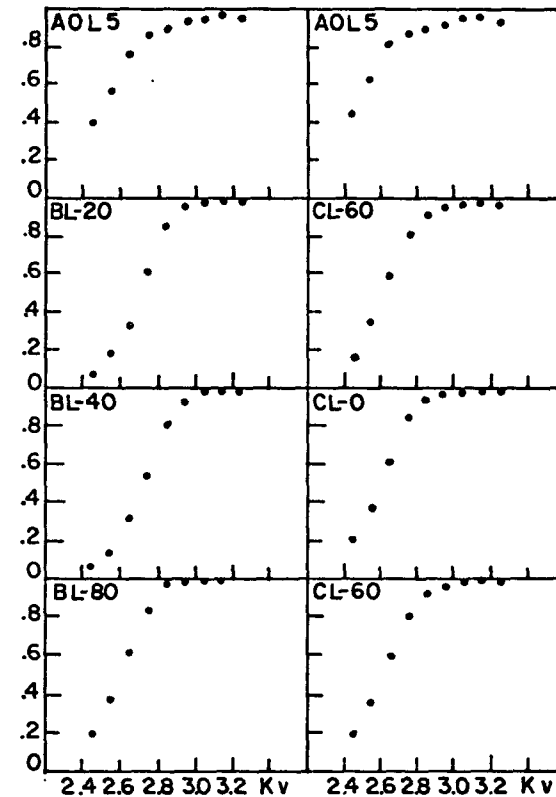
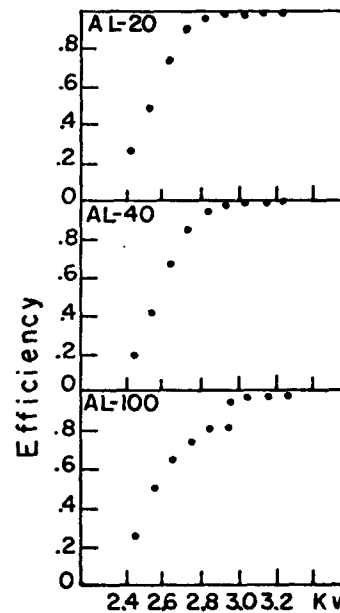
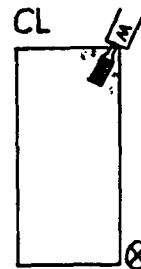
Fig. 2

a. Plan and side view of the C_0 counter shown in its location in the experiment.
 b. Mapping of the efficiency of the C_e counter over its whole phase space. The letters on the plot refer to efficiencies measured for trajectories between the corresponding points marked on the grid at each end of the counter.
 c. Pulse height spectrum from the photo tube (RCA C31000M) of the C_0 Cerenkov counter. Clearly visible are the one, two or three photoelectron peaks.

Configuration Of Wire Planes In Proportional Chambers



RUN 44
 CHAMBER CL
 SET: low P
 TARGET: 9 x Be
 PULSE: 4 x 10⁴
 EVENTS: 1000
 G2 RATE: 10/PULSE
 TRIG: G1=DX
 G2=RIGHTWI-TYEST

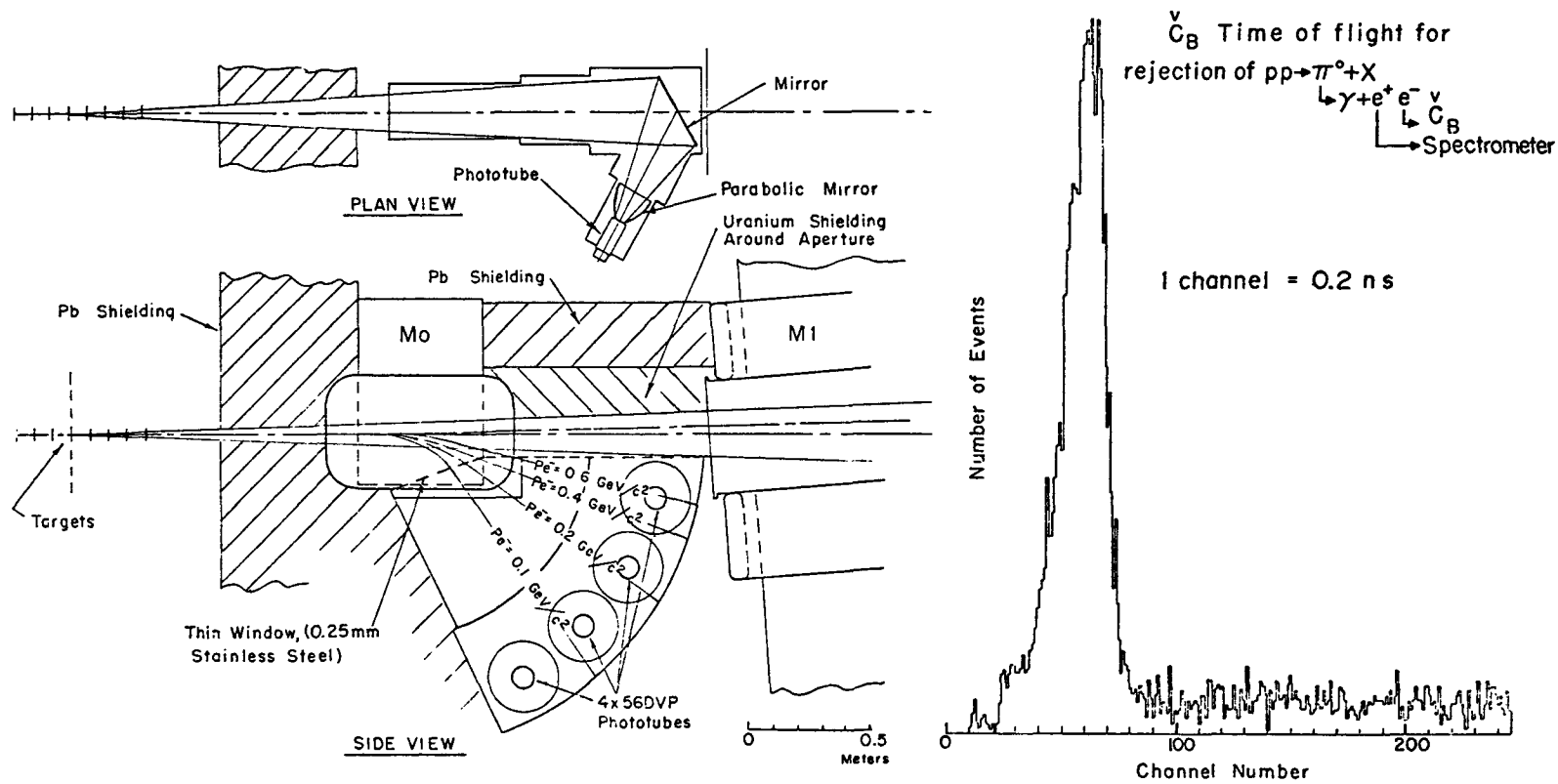


a

b

Fig 3

- (a) Relative orientation of the planes of wires in the proportional chambers.
- (b) Efficiency of all the wire planes as a function of the applied voltage. The position where this measurement was made is indicated by the sketch in the top left hand corner.



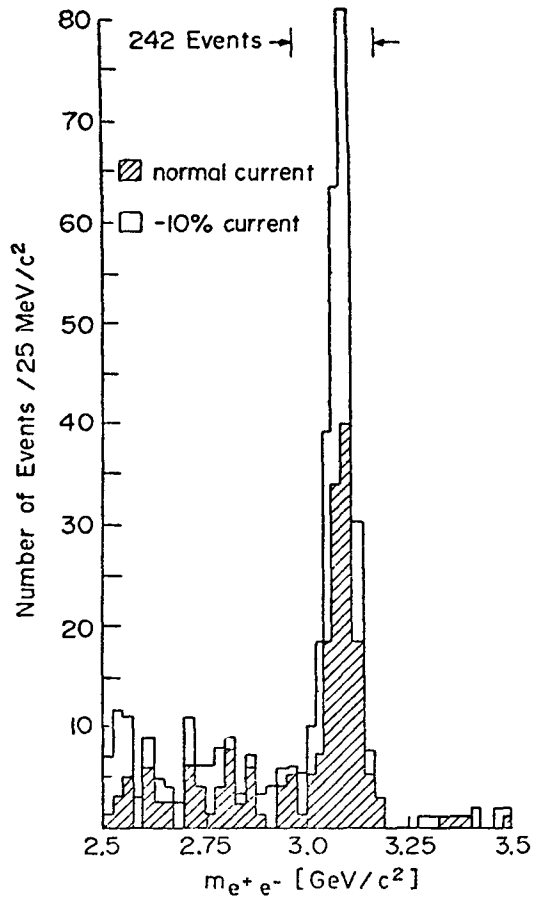
Plan and side view of the C_B counter shown in its location in the experiment

a

Relative timing between a pulse from the C_B counter and an electron trigger from the same spectrometer arm.

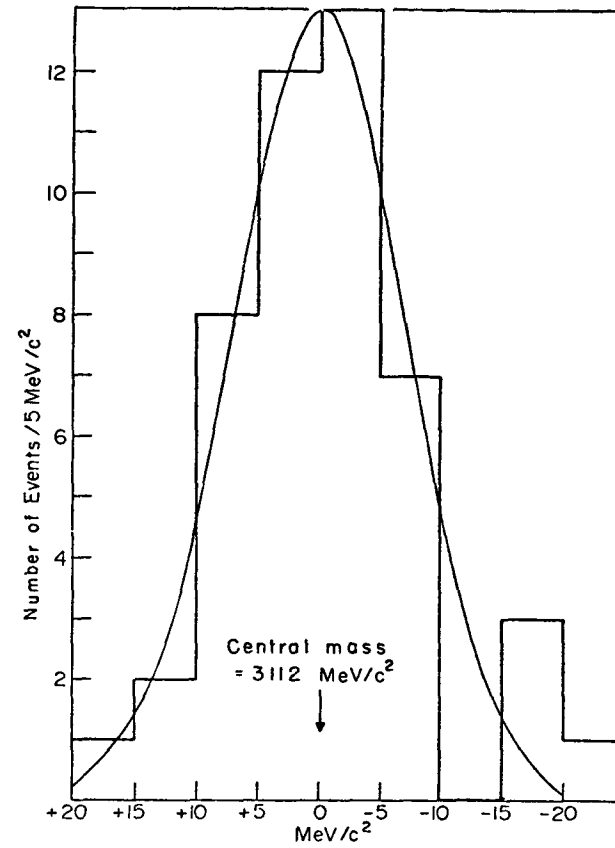
b

Fig 4



Mass spectrum for events in the mass range $2.5 < m_{ee} < 3.5$ GeV/c². The shaded events correspond to those taken at the normal momentum setting, while the unshaded ones correspond to a momentum setting 10% below normal. The acceptance is a smooth function of m .

a



The width of J

b

Fig 5

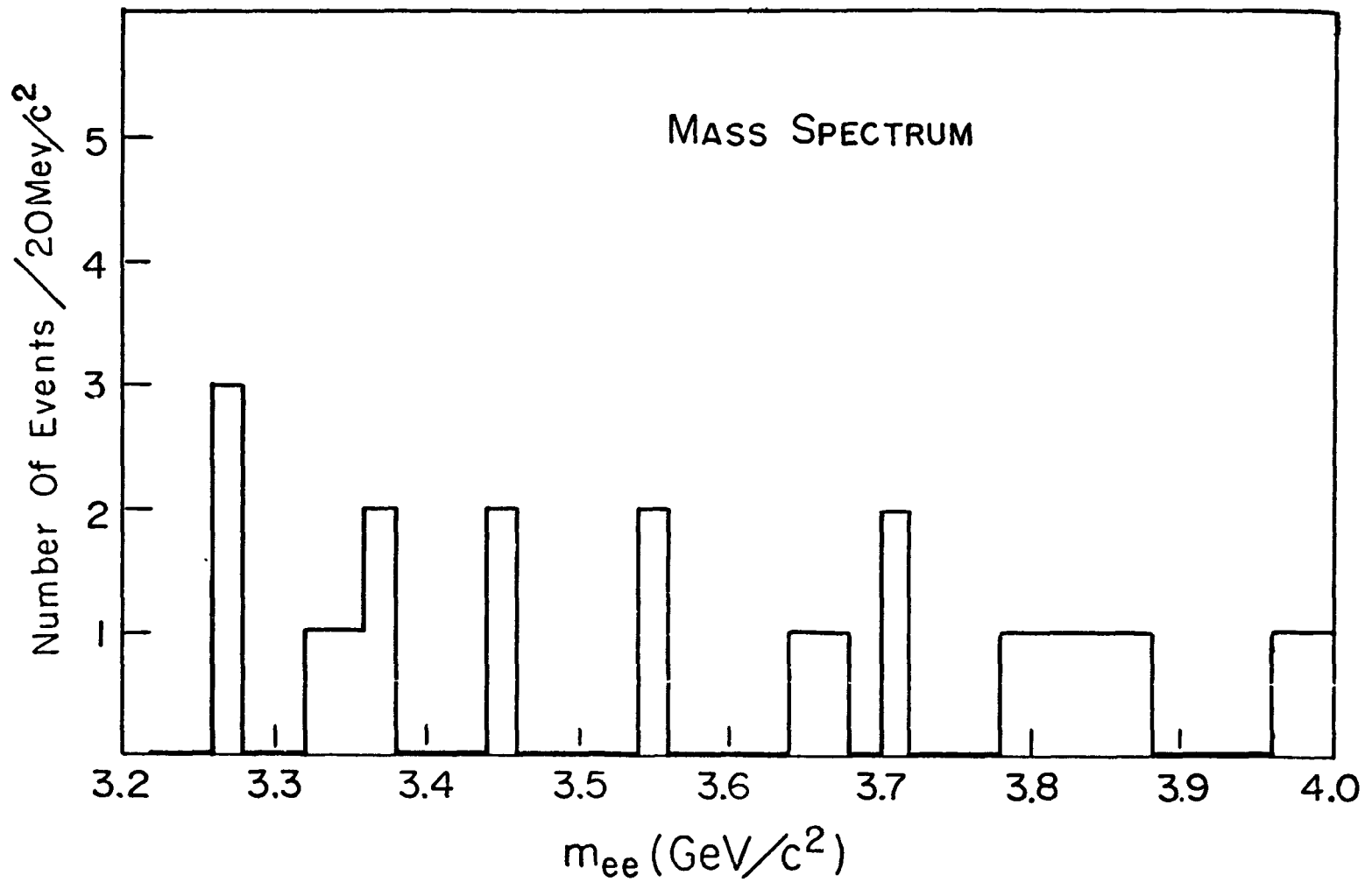
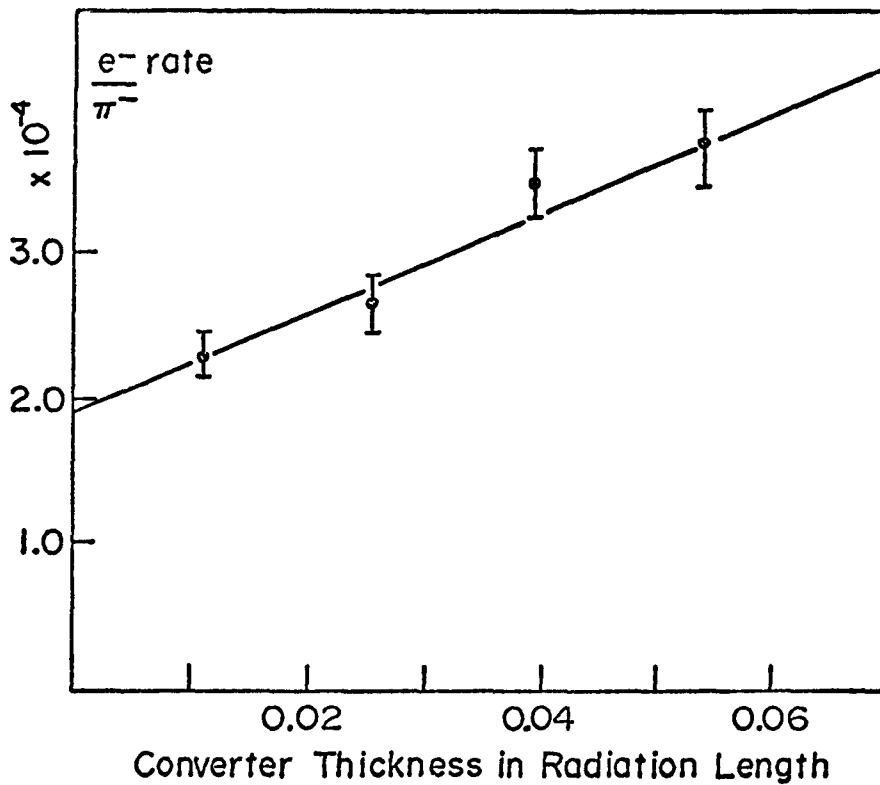
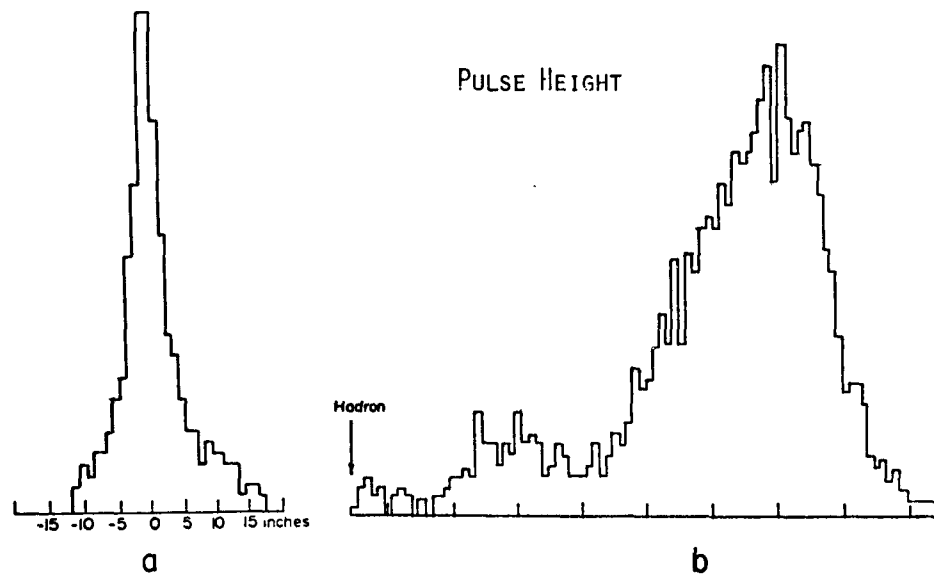


Fig. 6

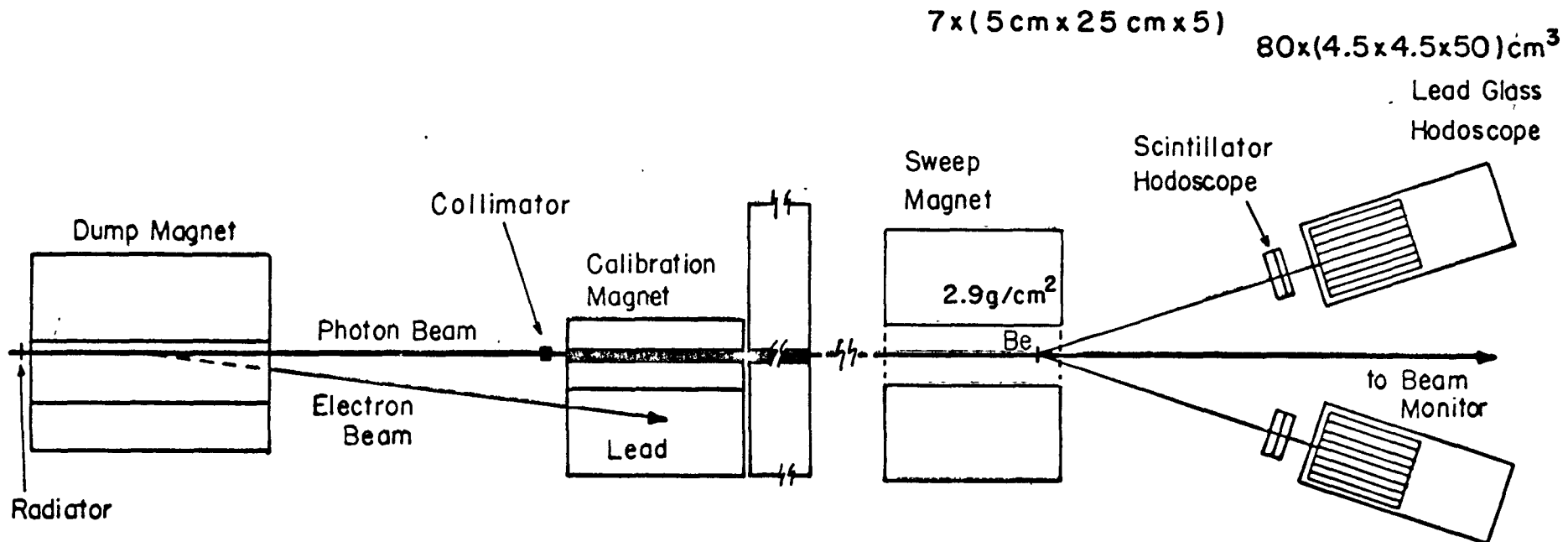
Mass spectrum for events in the mass range $3.2 < m_{ee} < 4.0$ GeV/c², normalized to fig. 5a.

TARGET RECONSTRUCTION



c
Fig.7

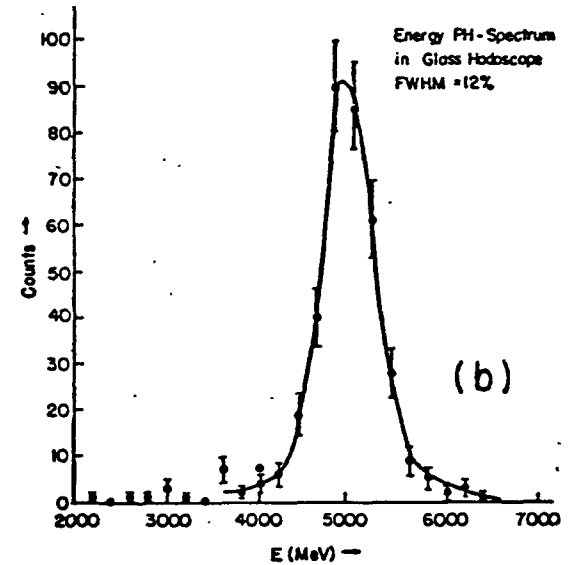
- a. Target reconstruction for single arm e^- events, with one piece of target.
- b. Pulse height in the shower counters for single arm e^- events.
- c. e^-/π^- rate in one arm as a function of thickness of converter placed between the target and the spectrometer arm.



(a) Side View

Incident energy 11.8 GeV
 Intensity: 2×10^{11} EQ/min
 $\frac{\delta E}{E} = \frac{12}{\sqrt{E}}$ rms $\delta s = 0.5$ cm
 Trigger $E_{1,2} > 2.5$ $E_1 + E_2 > 7.0$

Fig. 8



- (a) Cornell photoproduction pair spectrometer
- (b) Energy resolution of lead glass hodoscope.

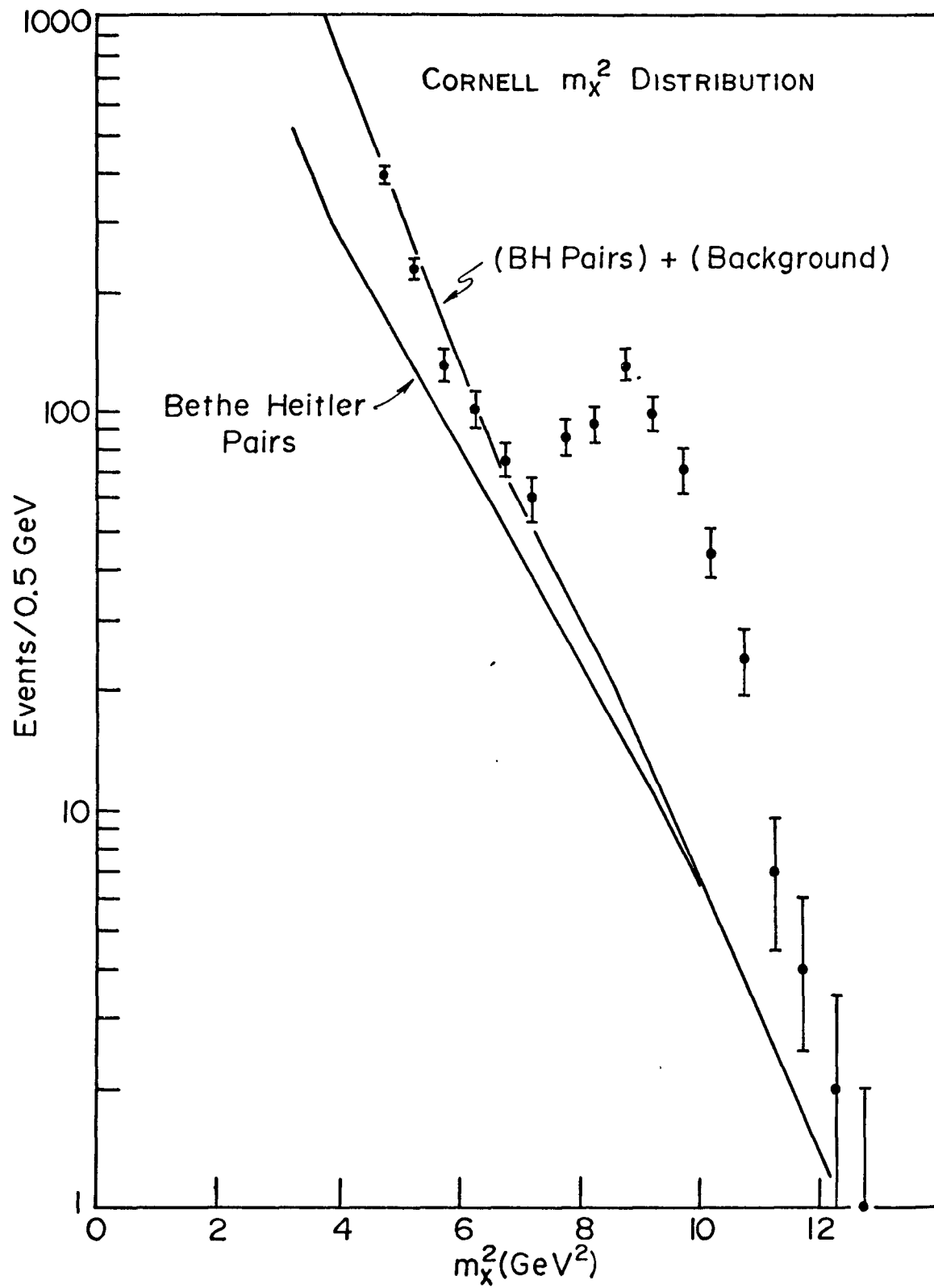
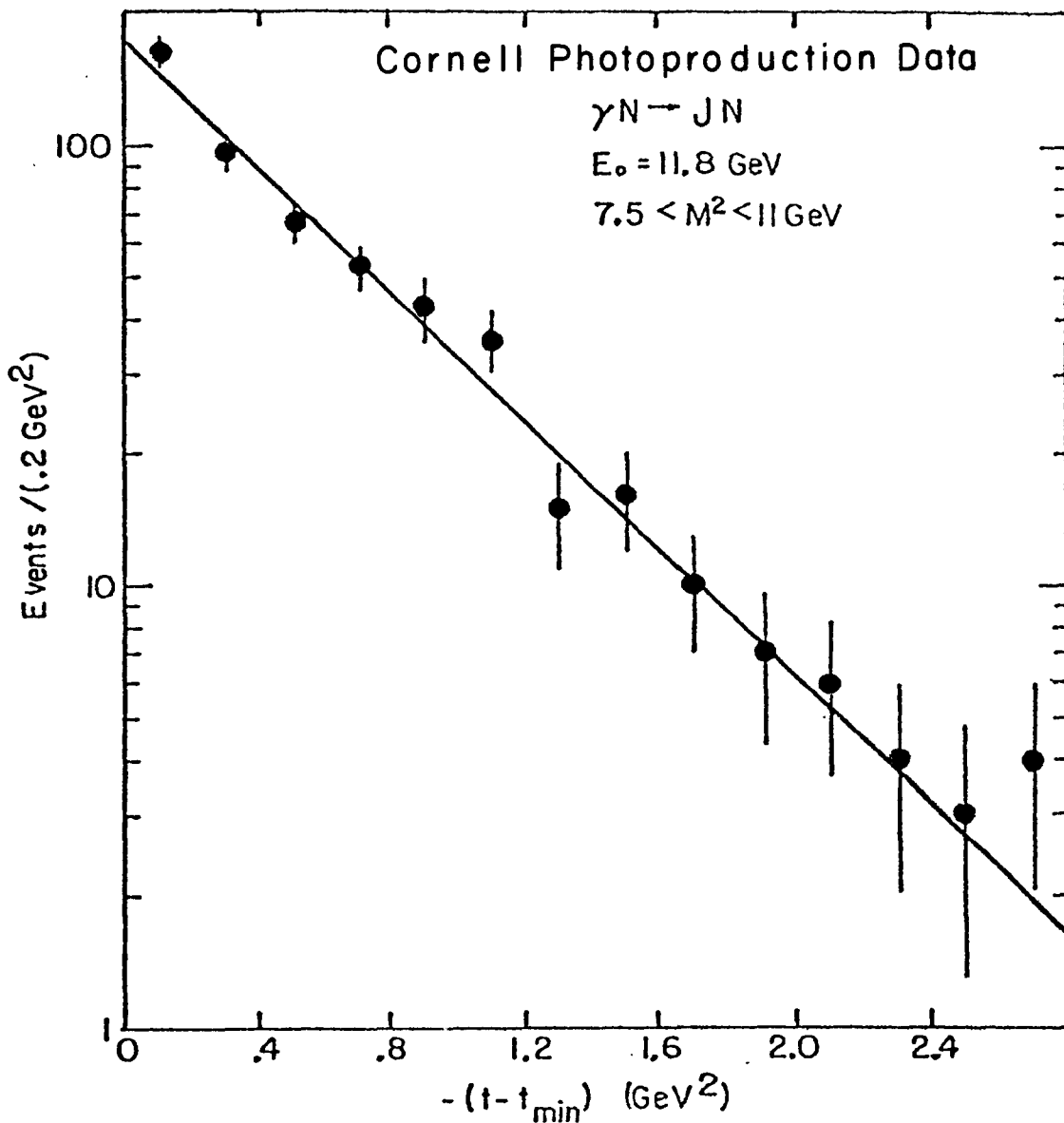


Fig. 9

Event distribution versus mass squared of pairs in the Cornell apparatus.

fit to: $(0.8 \pm 0.2)e^{-(1.2 \pm 0.3)t}$ nb/GeV²



The $t-t_{\min}$ distribution. The Solid line is calculated with $\frac{d\sigma}{dt} = (0.8 \pm 0.2)e^{-(1.2 \pm 0.3)t}$ nb/GeV². by folding in the Acceptance and j decay.

Fig. 10

Wisconsin-SLAC

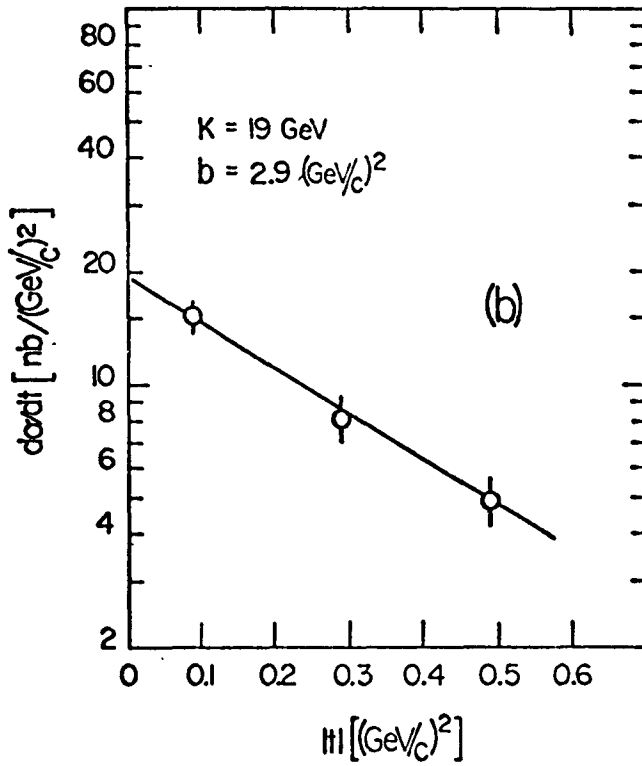
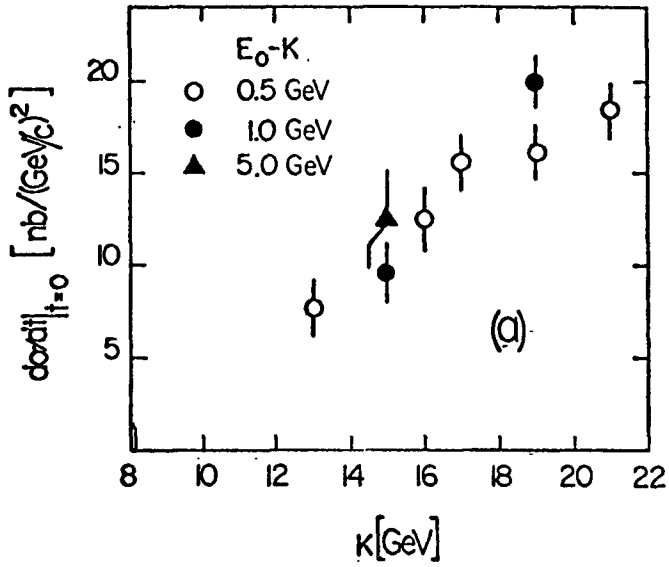


Fig. 11

- (a) Cross section extrapolated to $t=0$ for J as a function of energy.
- (b) Differential cross section for J , for $K=19$ GeV and $E_0=20$ GeV as a function of t .

P1-4: proportional chambers
 M2 : magnet, aperture 40.6 x 61 cm, vertical bending 20 kG·m
 e : shower counters
 H : hadron calorimeter
 μ : μ counter

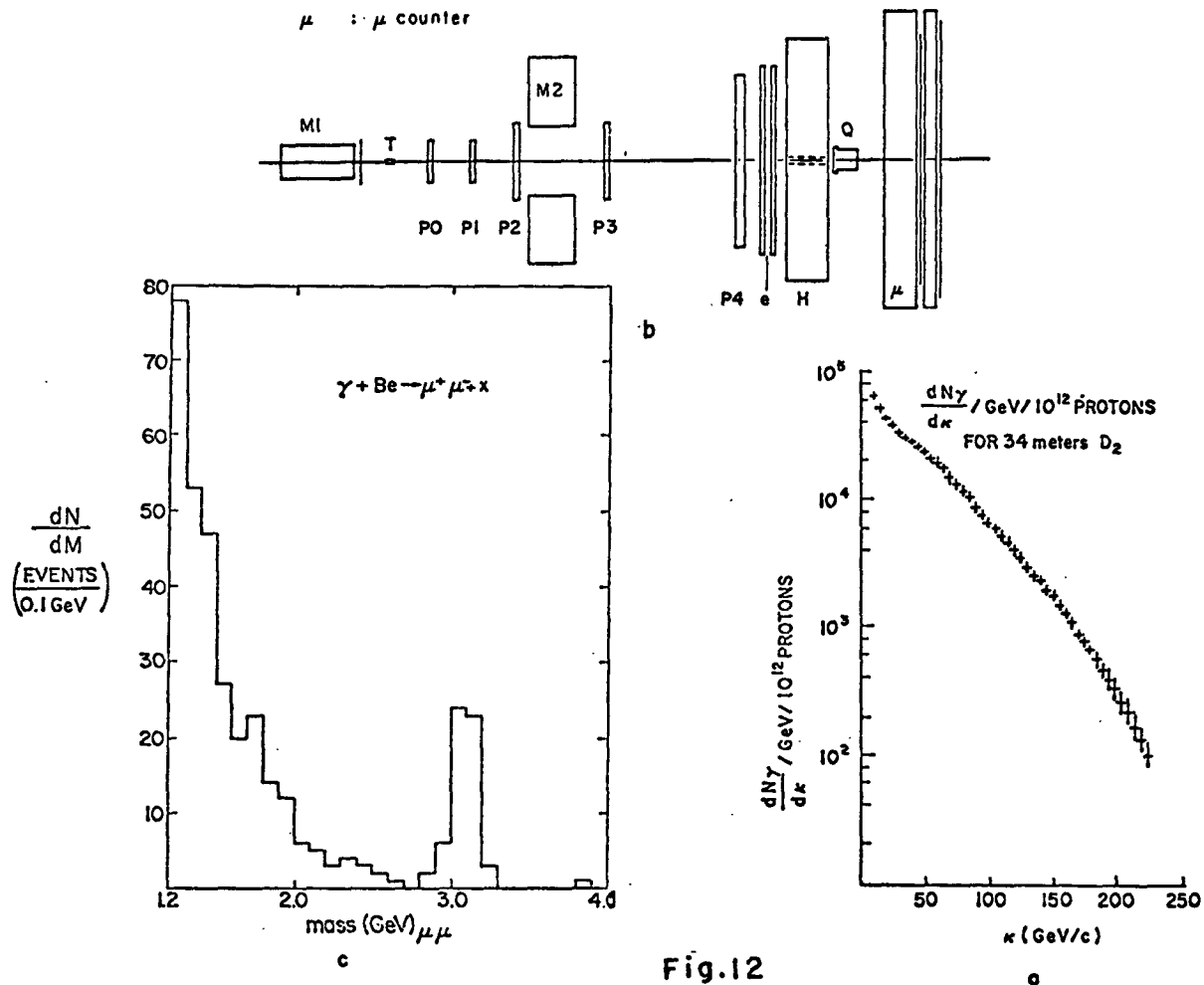


Fig.12

Photoproduction of J at Fermilab.

- (a) Photon energy spectrum observed at photon target with cryostat filled with liquid D_2 .
- (b) Layout of detectors in the experimental enclosure.
- (c) Dimuon invariant mass distribution observed above 1.2 GeV.

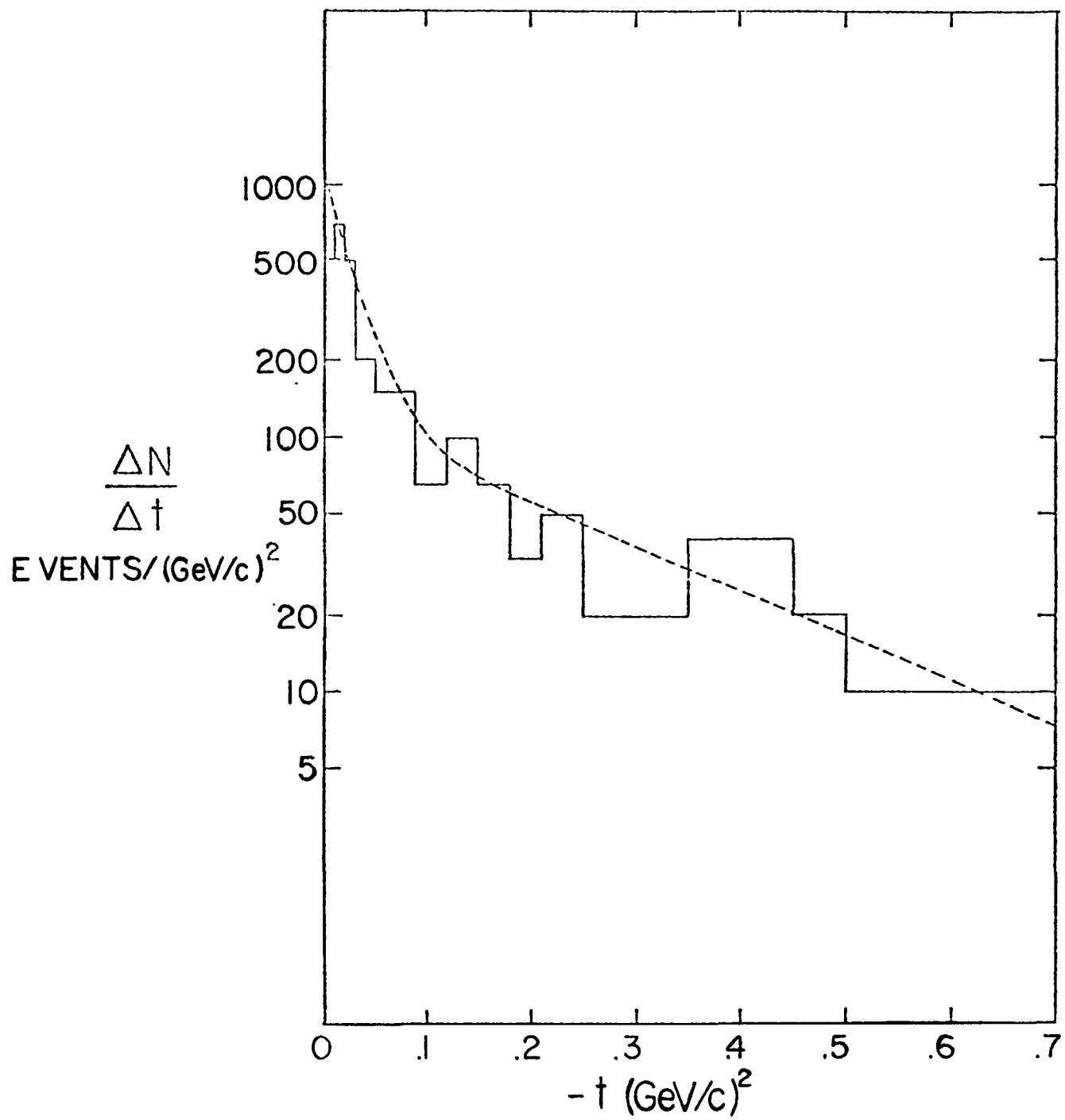


Fig.13

t distribution observed at Fermilab for events in the 3.1 GeV peak of Fig. 12c.

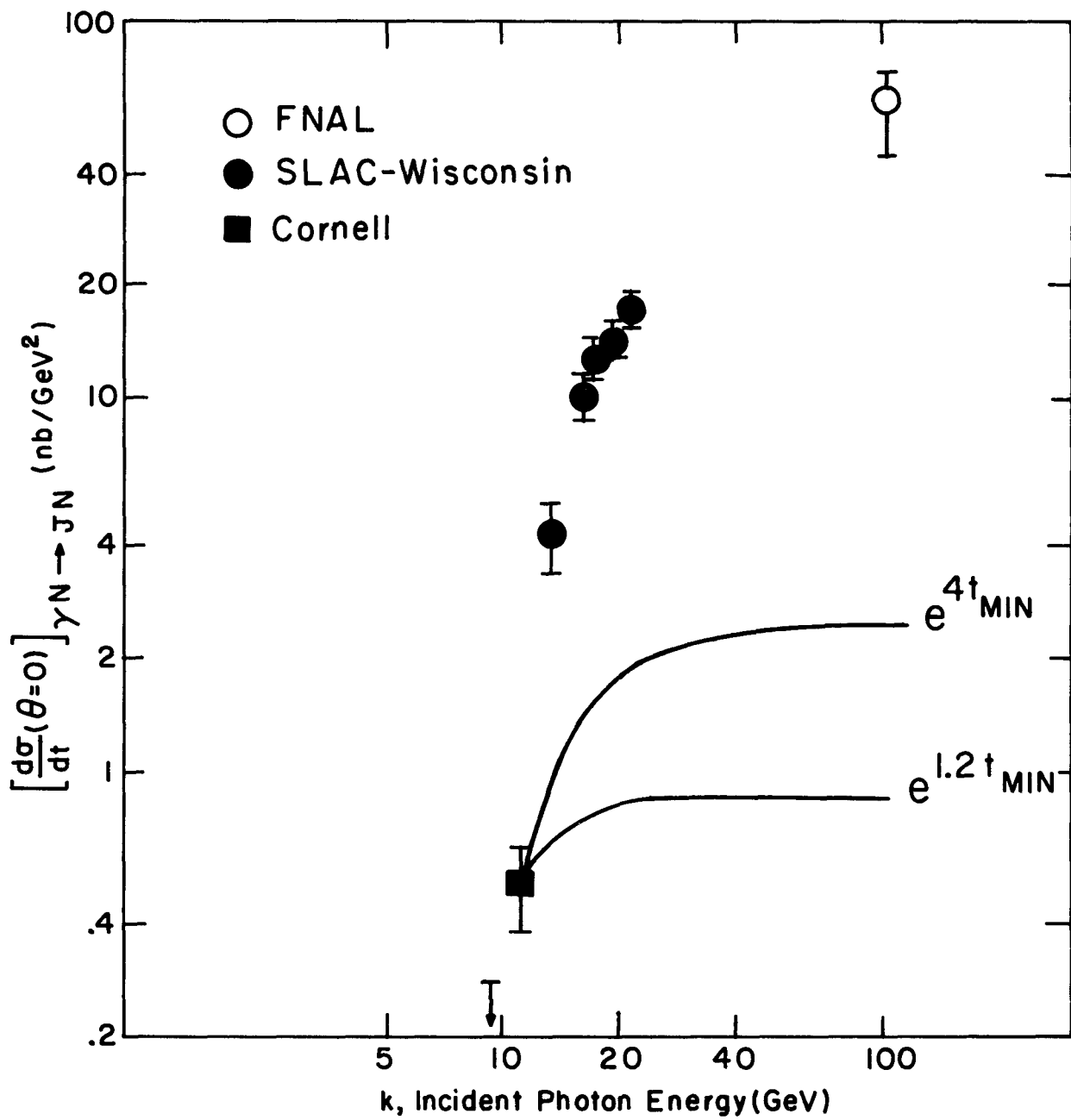


Fig. 14

Forward cross section as function of energy.

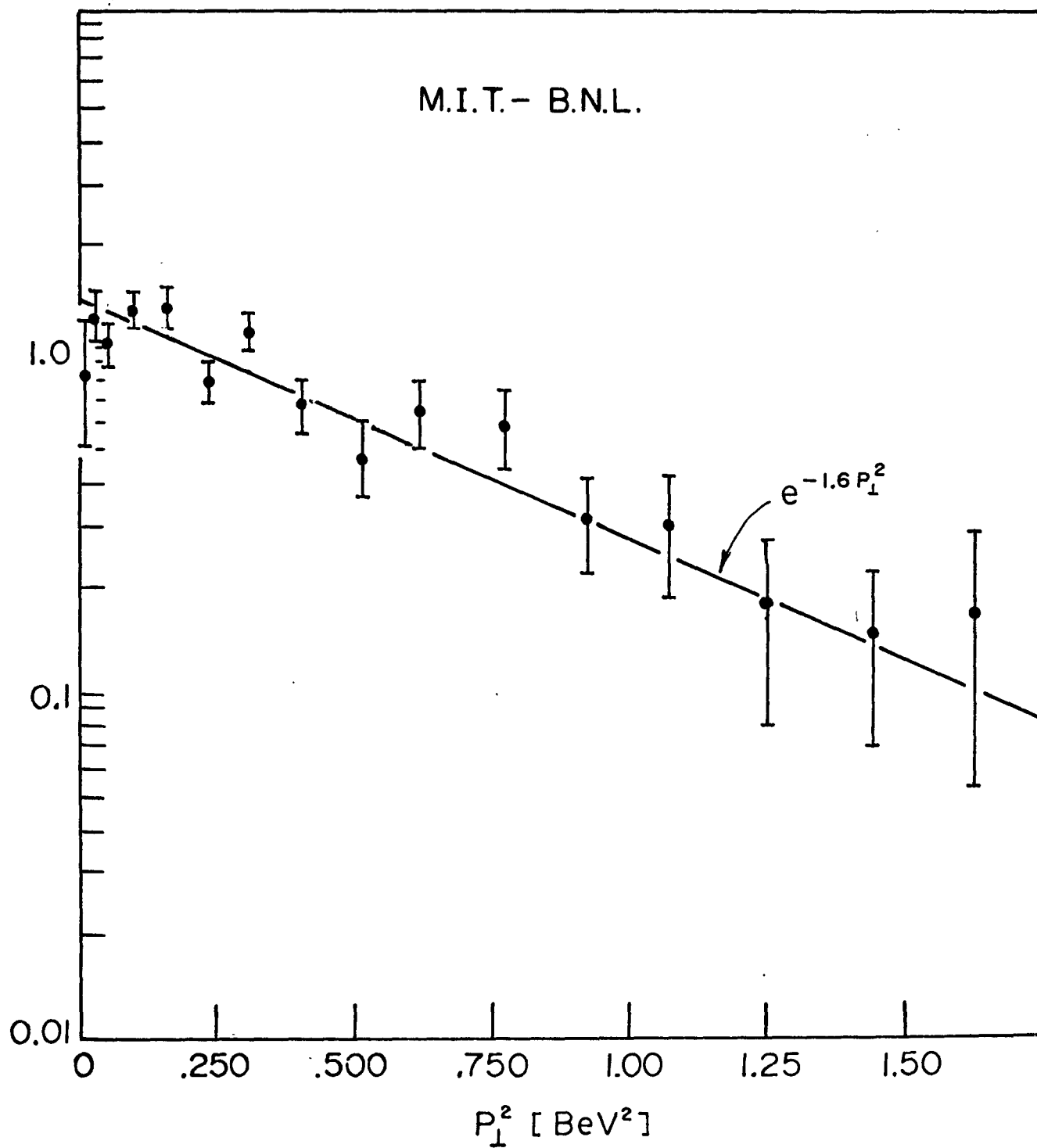


Fig. 15

Preliminary data of P_{\perp} dependence of J's produced on beryllium with a 30 GeV. proton beam, as measured by the MIT-BNL group.

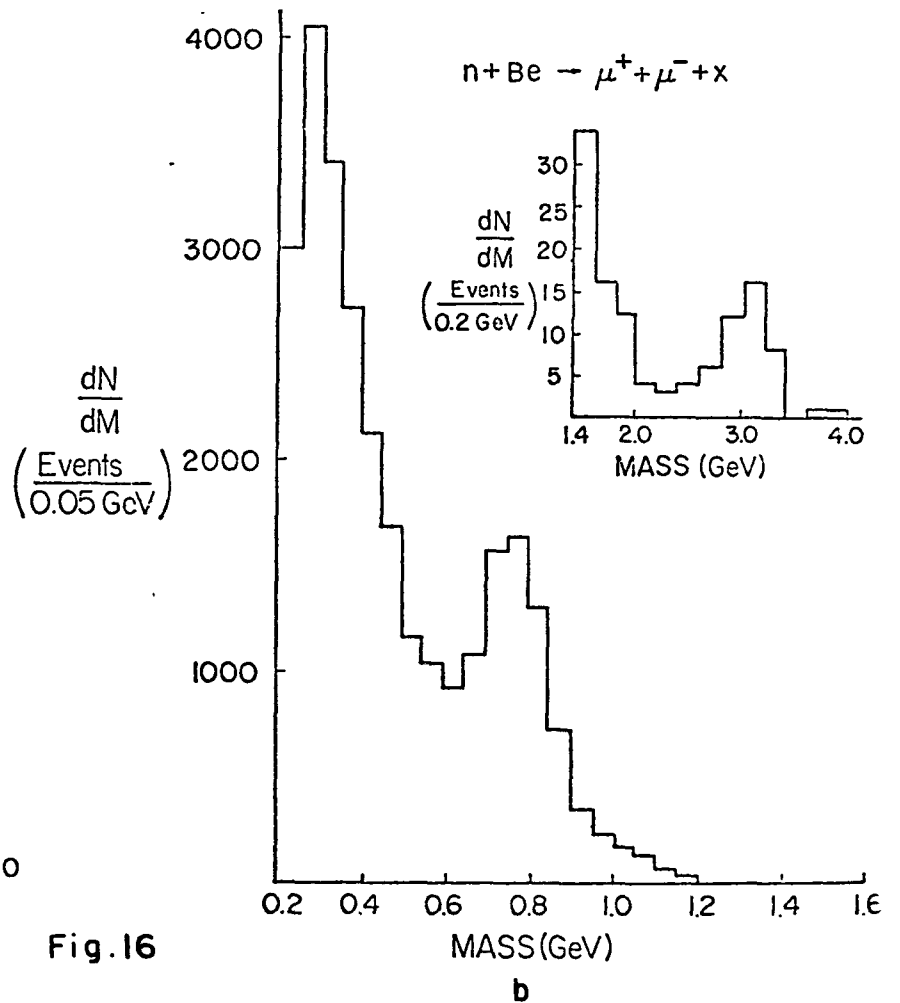
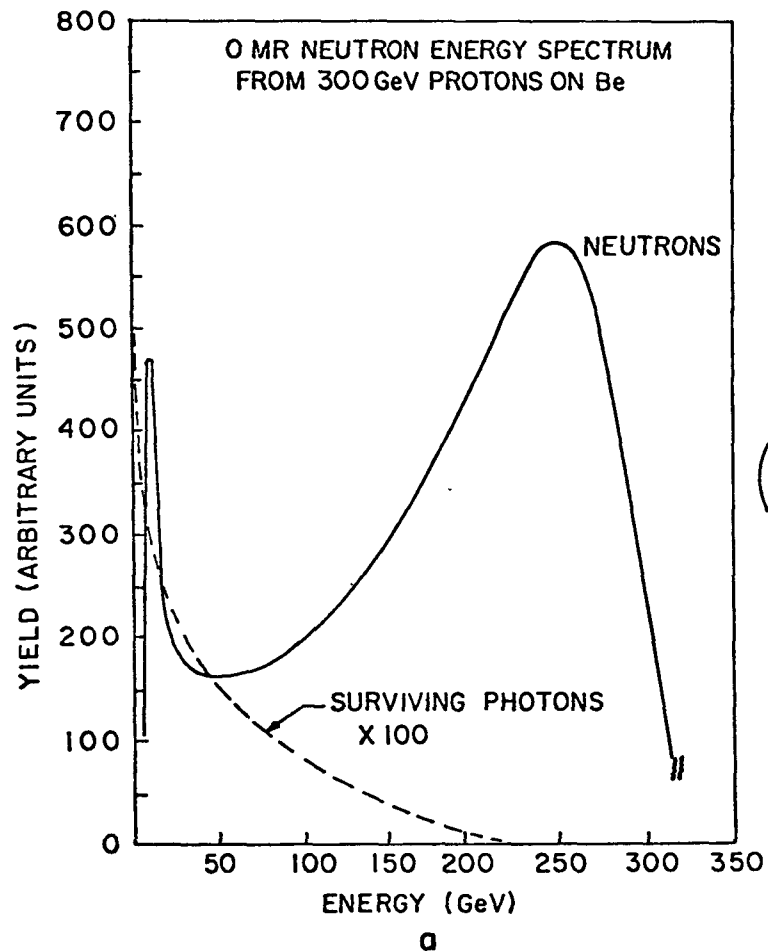


Fig.16

- (a) Neutron energy spectrum (raw distribution of neutron calorimeter pulse height) with the spectrum of surviving photons superimposed.
- (b) Invariant mass distribution of pairs of muons with opposite charge and total energy greater than 70 GeV.

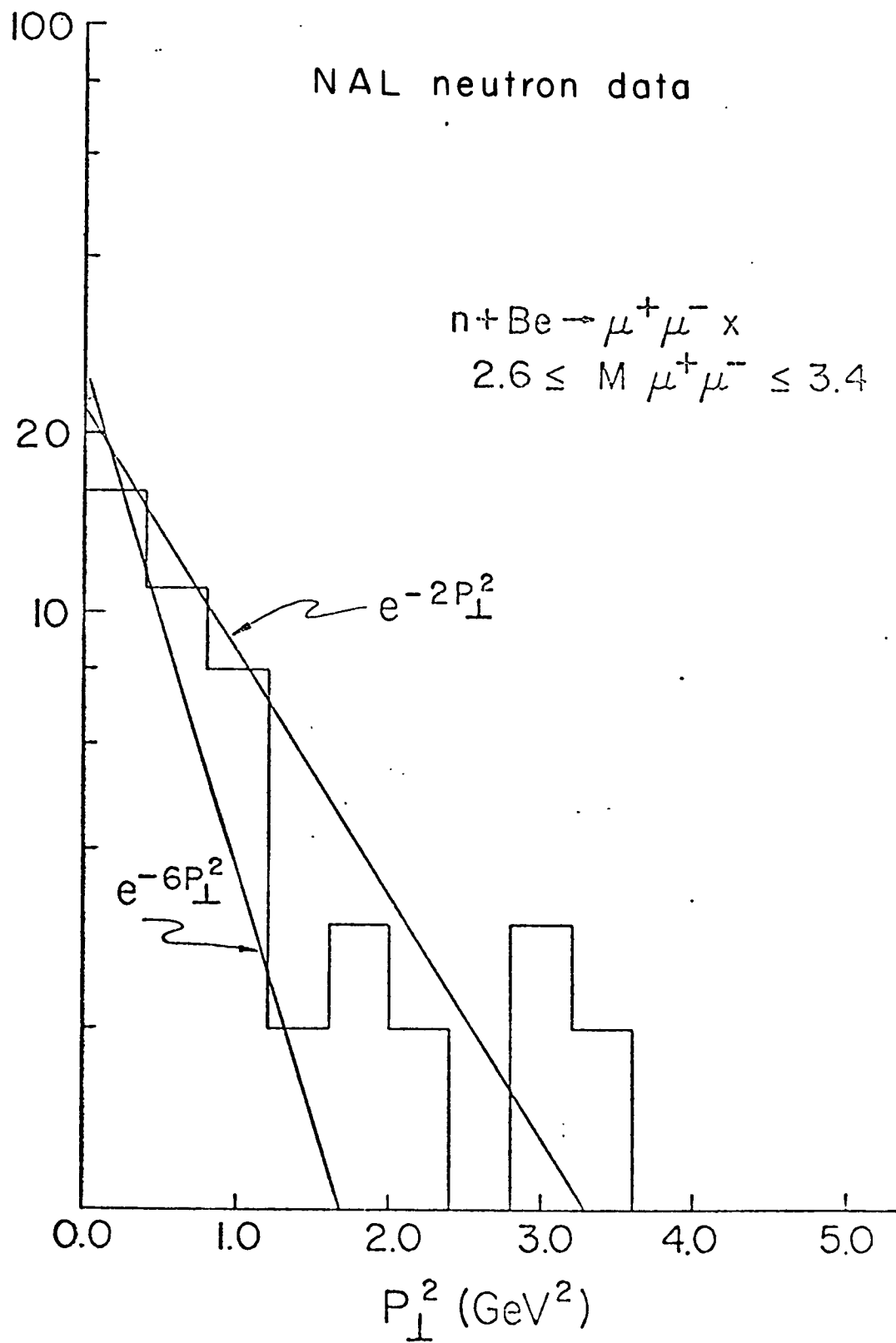


Fig. 17

P_{\perp} dependence of $J \rightarrow \mu^+ \mu^-$ produced by 250 GeV neutrons on Be at Fermilab.

I.S.R. (DI LELLA GROUP)

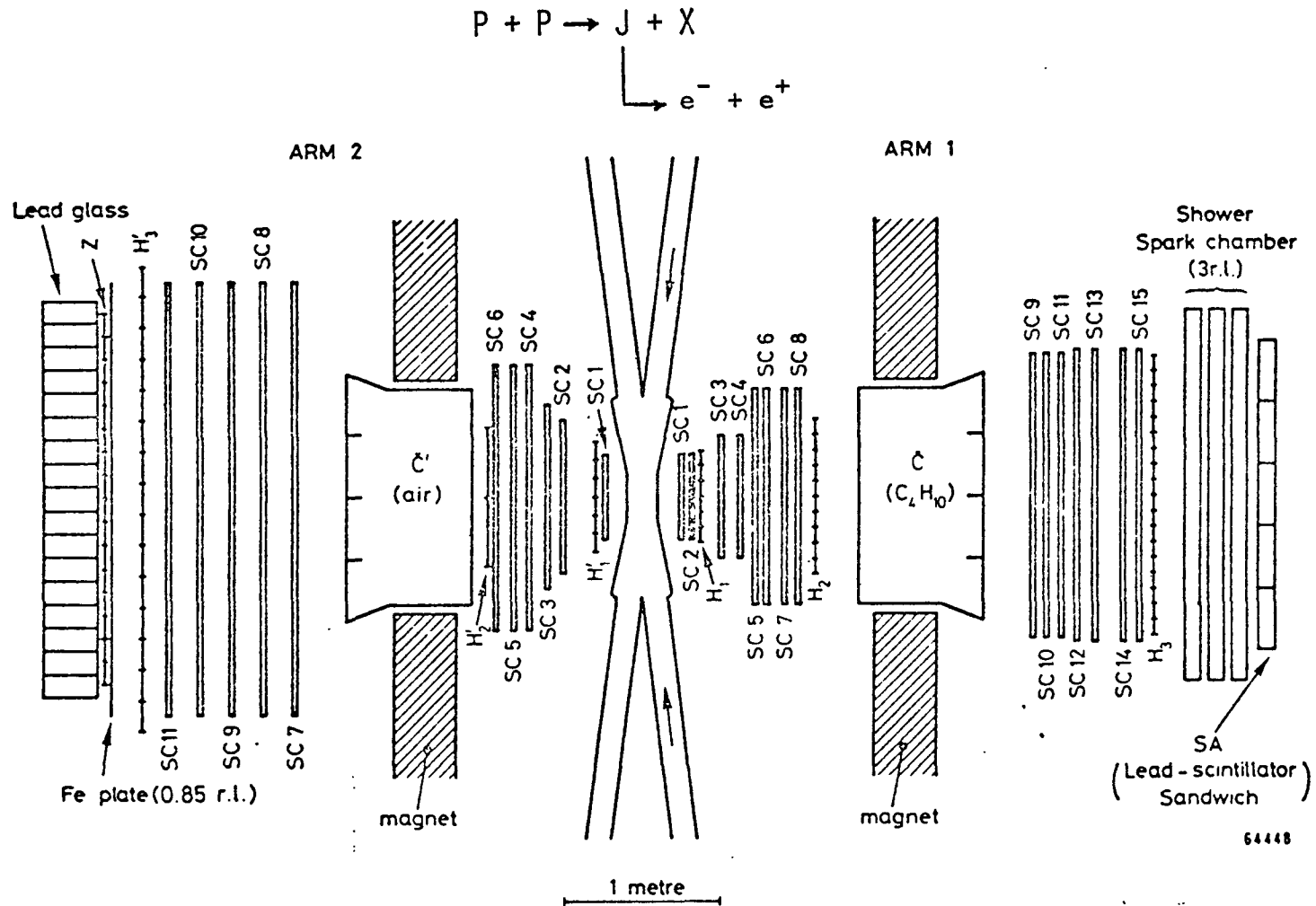
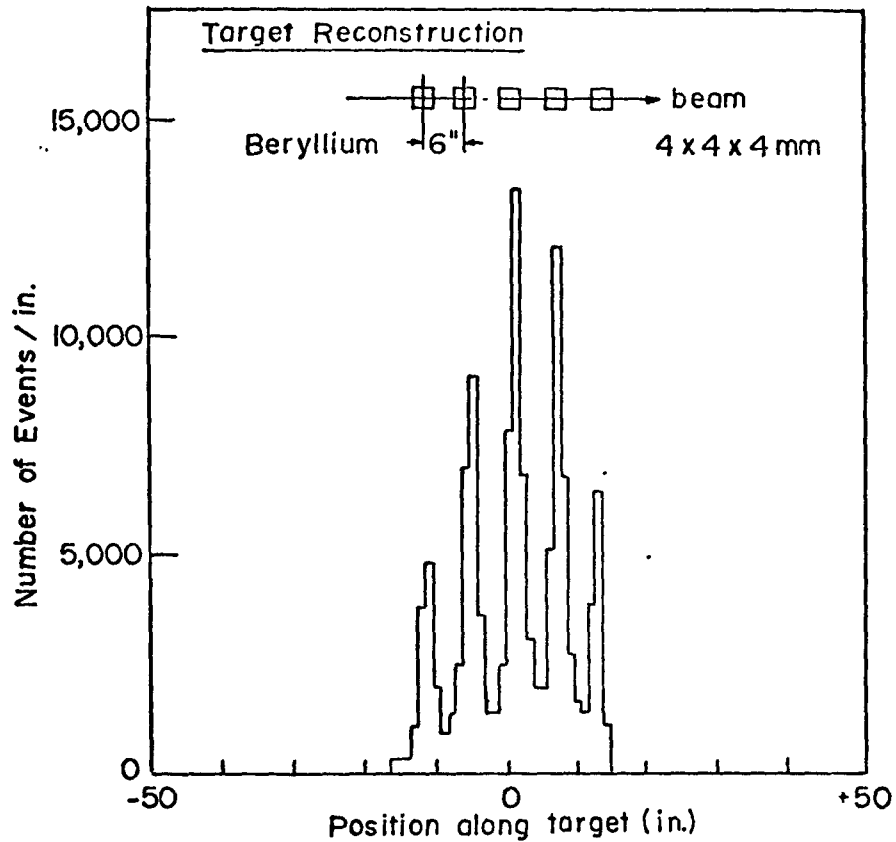
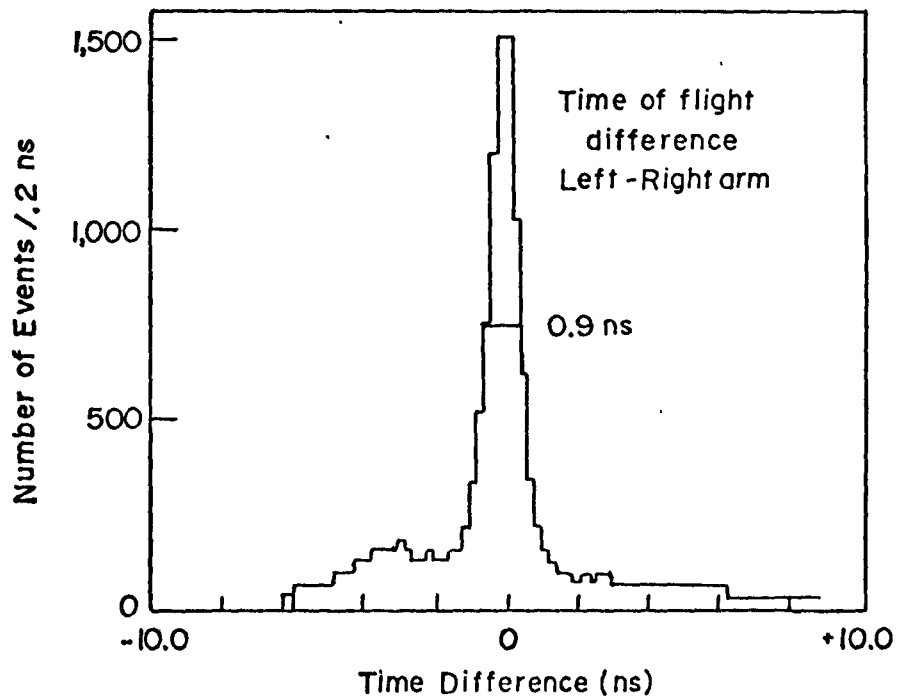


Fig.18

Plan view of the electron pair spectrometer at Il of the CERN Intersecting Storage Rings.



a. Reconstruction of the pair vertex at the target; using information from the proportional chambers. The five pieces of beryllium are seen clearly.



b. Time difference between additional scintillation counters in the left and right arms. The resolution obtained is 0.9 ns and little background is present.

Fig. 19

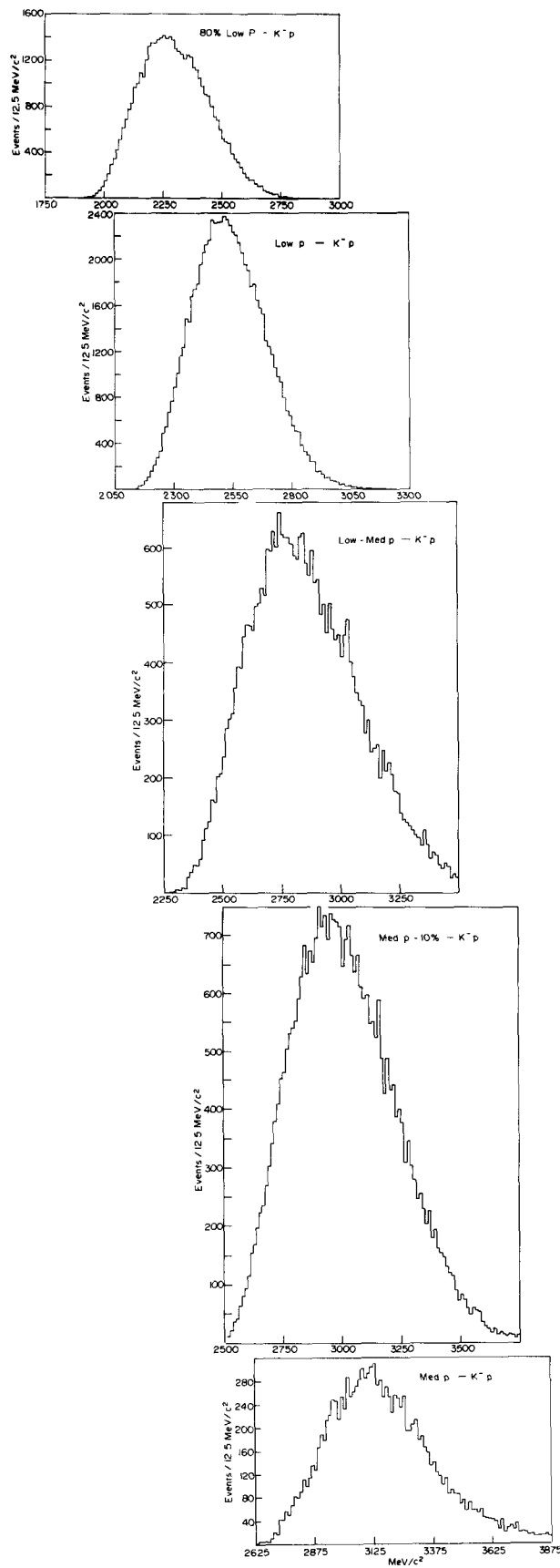


Fig. 20. $K^- p$ mass spectra for five mass ranges from MIT-BNL.

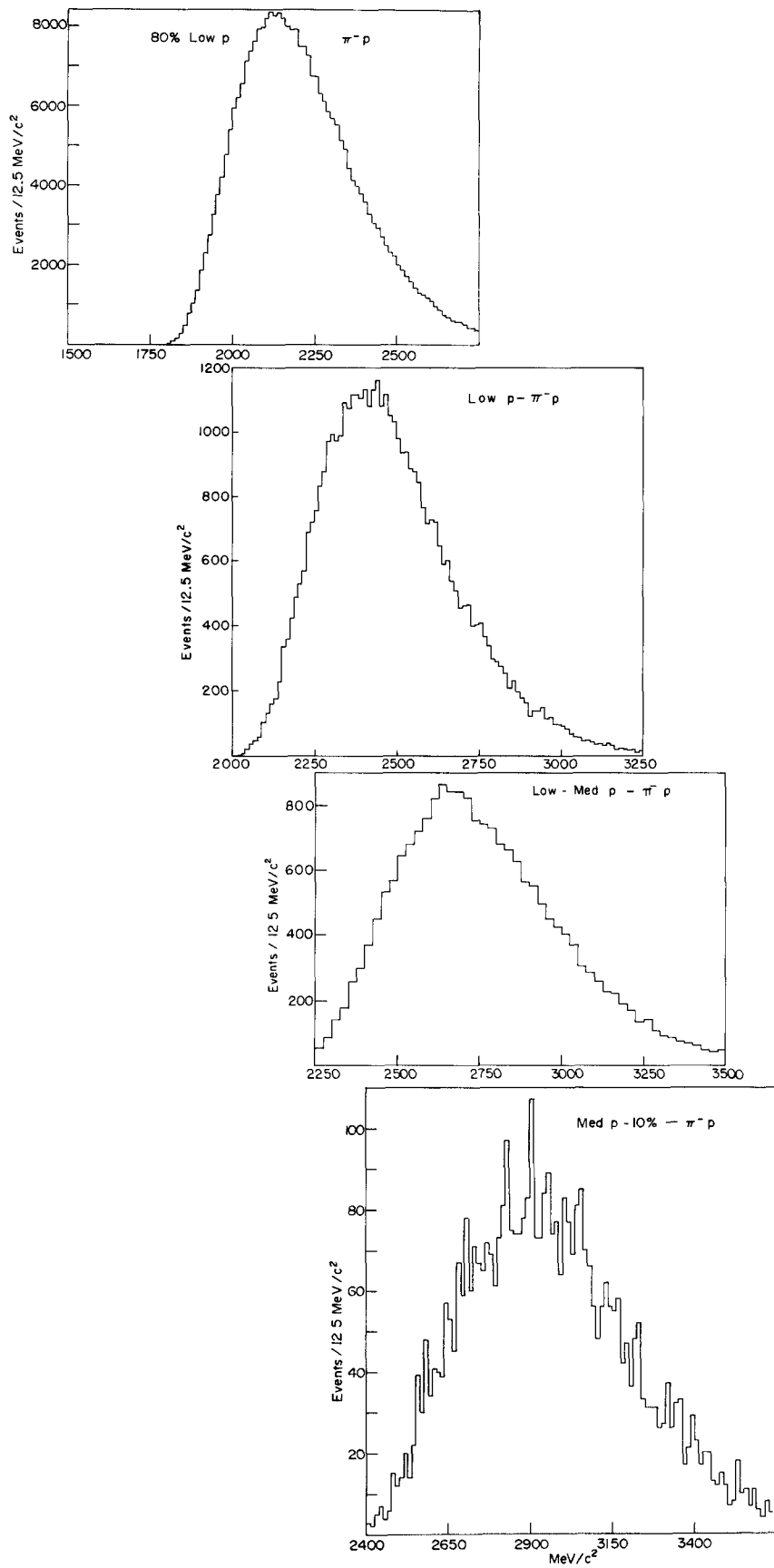


Fig. 21. $\pi^- p$ mass spectra for four mass ranges from MIT-BNL.

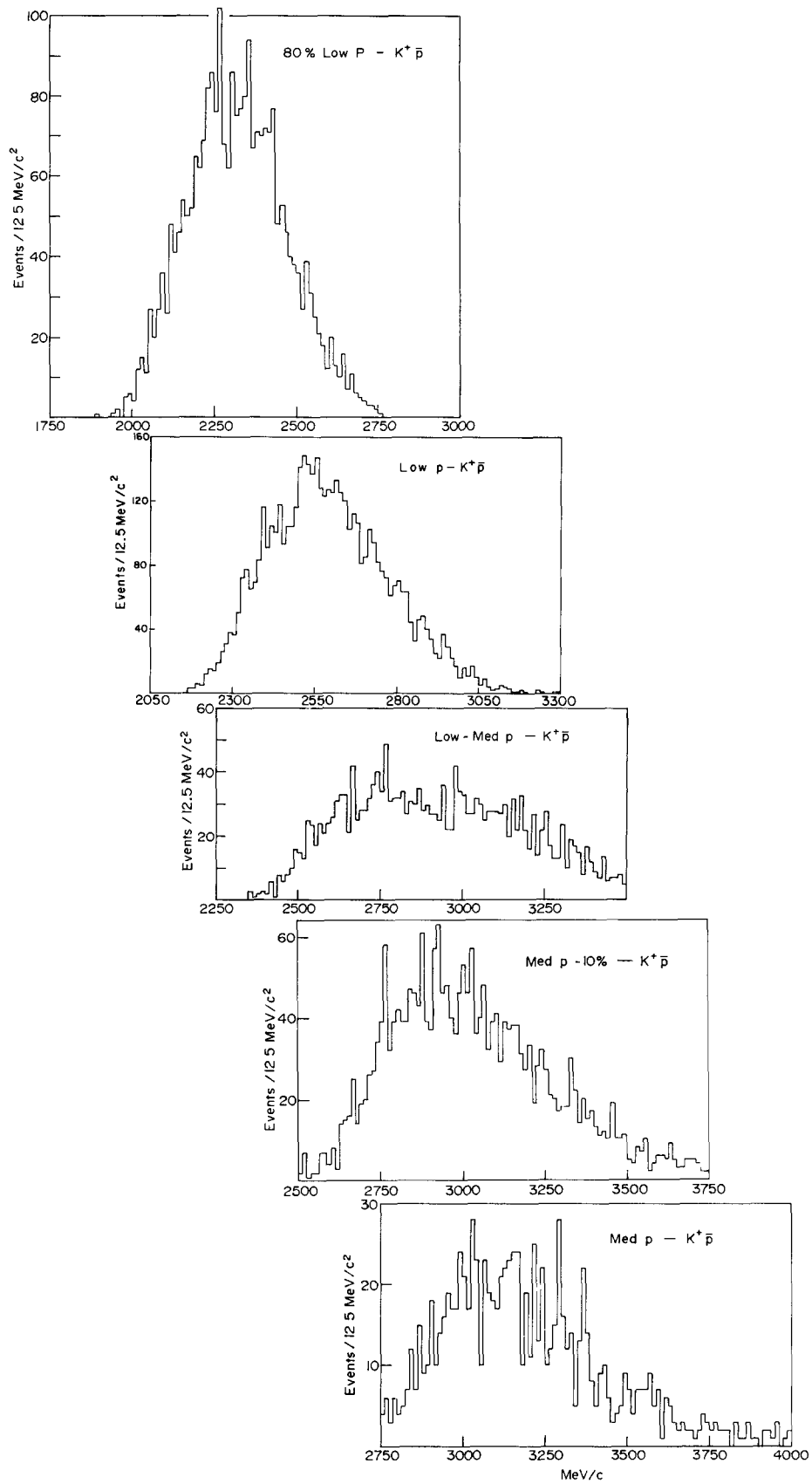


Fig. 22. $\bar{p} K^+$ mass spectra for five mass ranges from MIT-BNL.

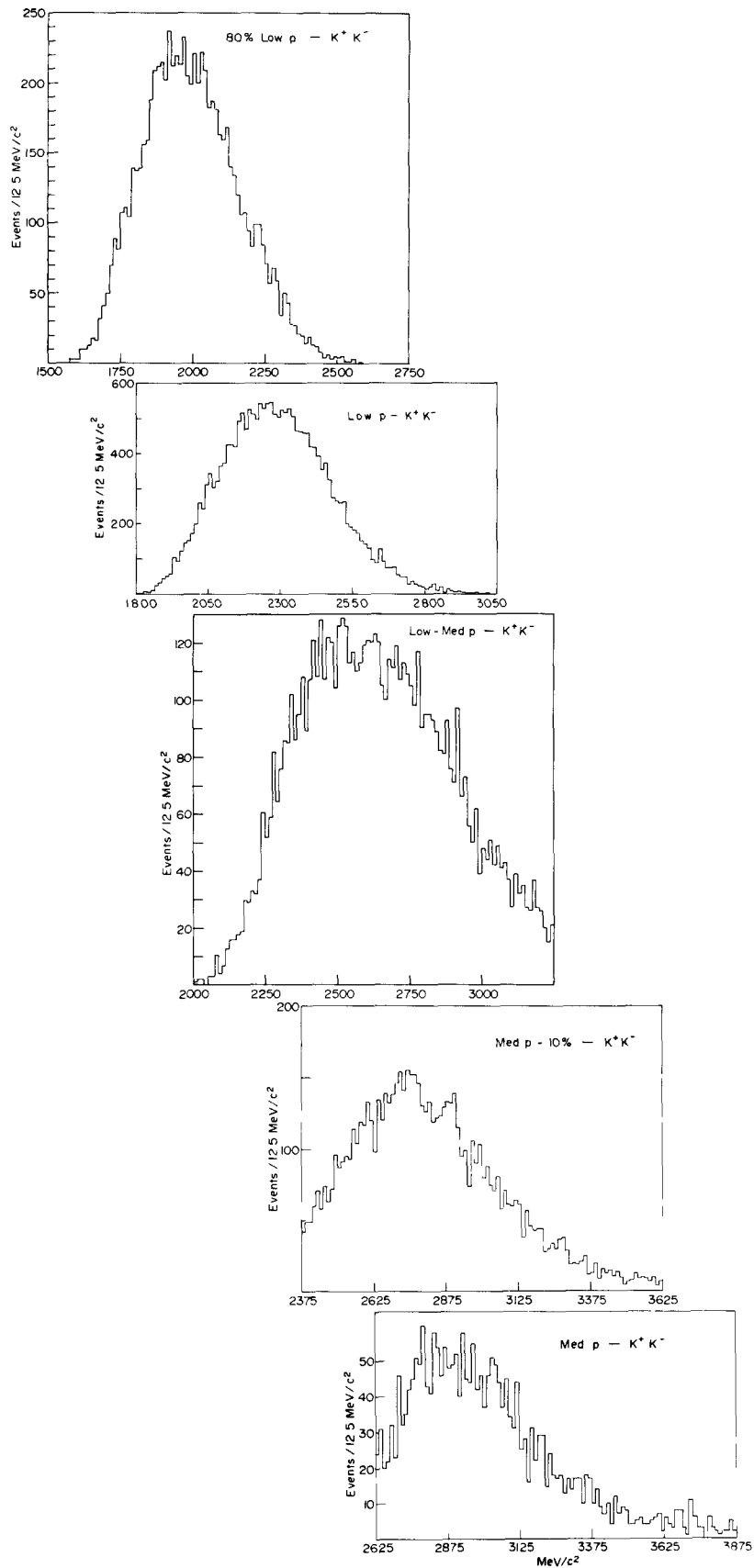


Fig. 23. K^+K^- mass spectra for five mass ranges from MIT-BNL.

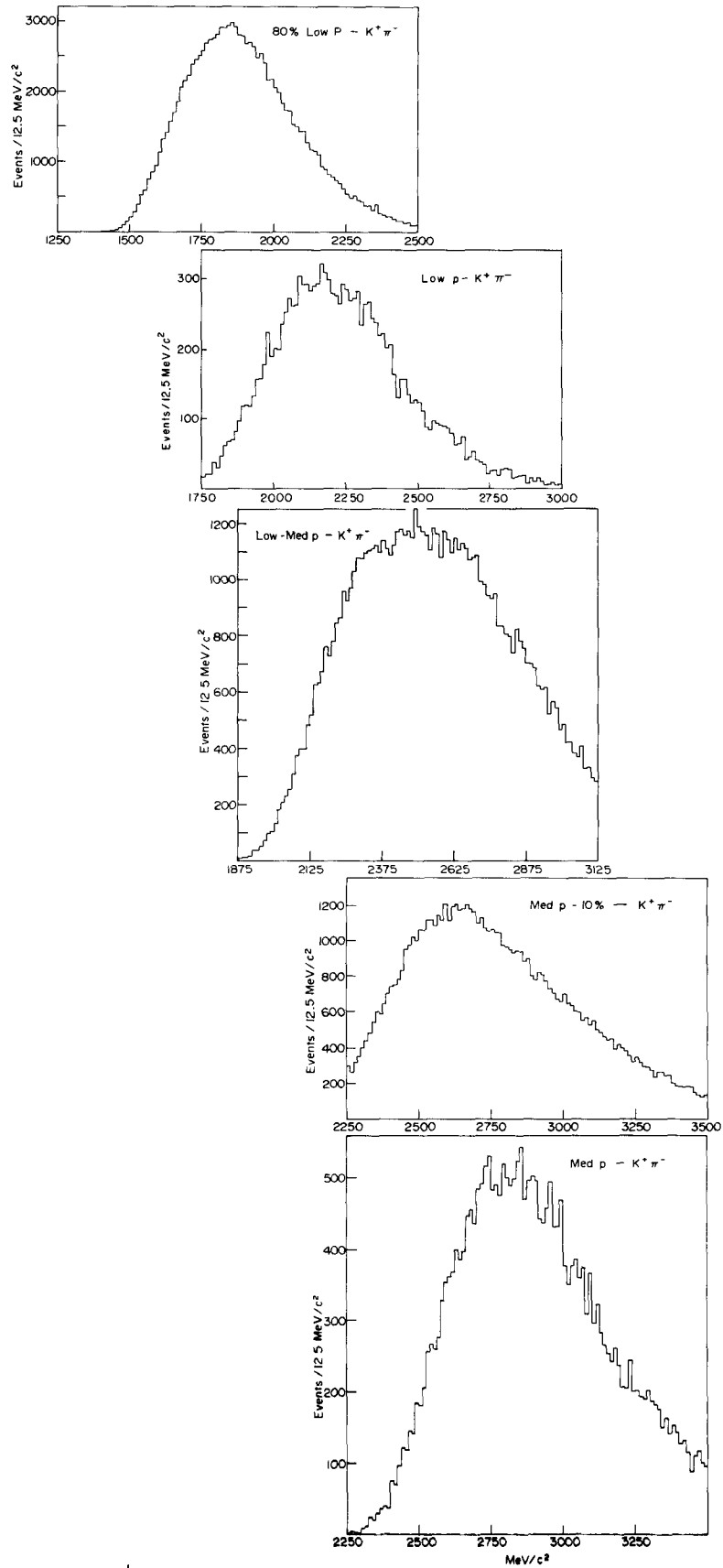


Fig. 24. $\pi^- K^+$ mass spectra for five mass ranges from MIT-BNL.

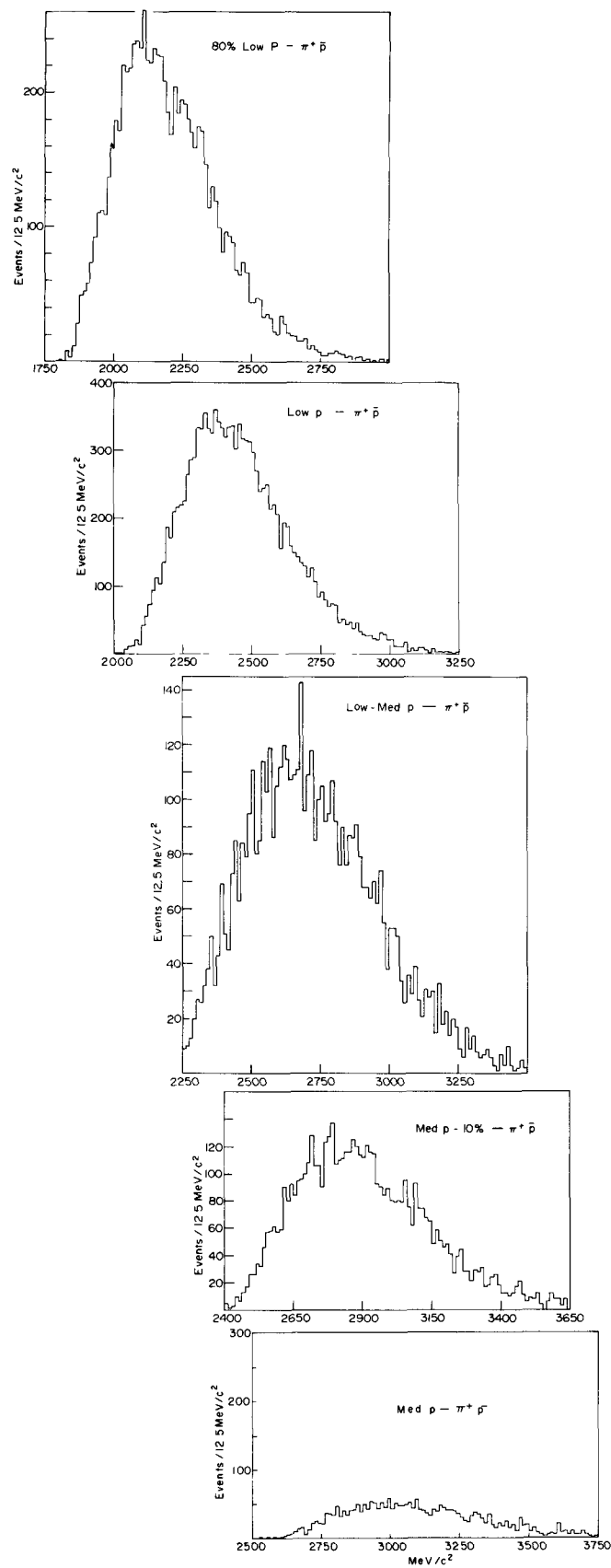


Fig. 25. $\bar{p} \pi^+$ mass spectra for five mass ranges from MIT-BNL.

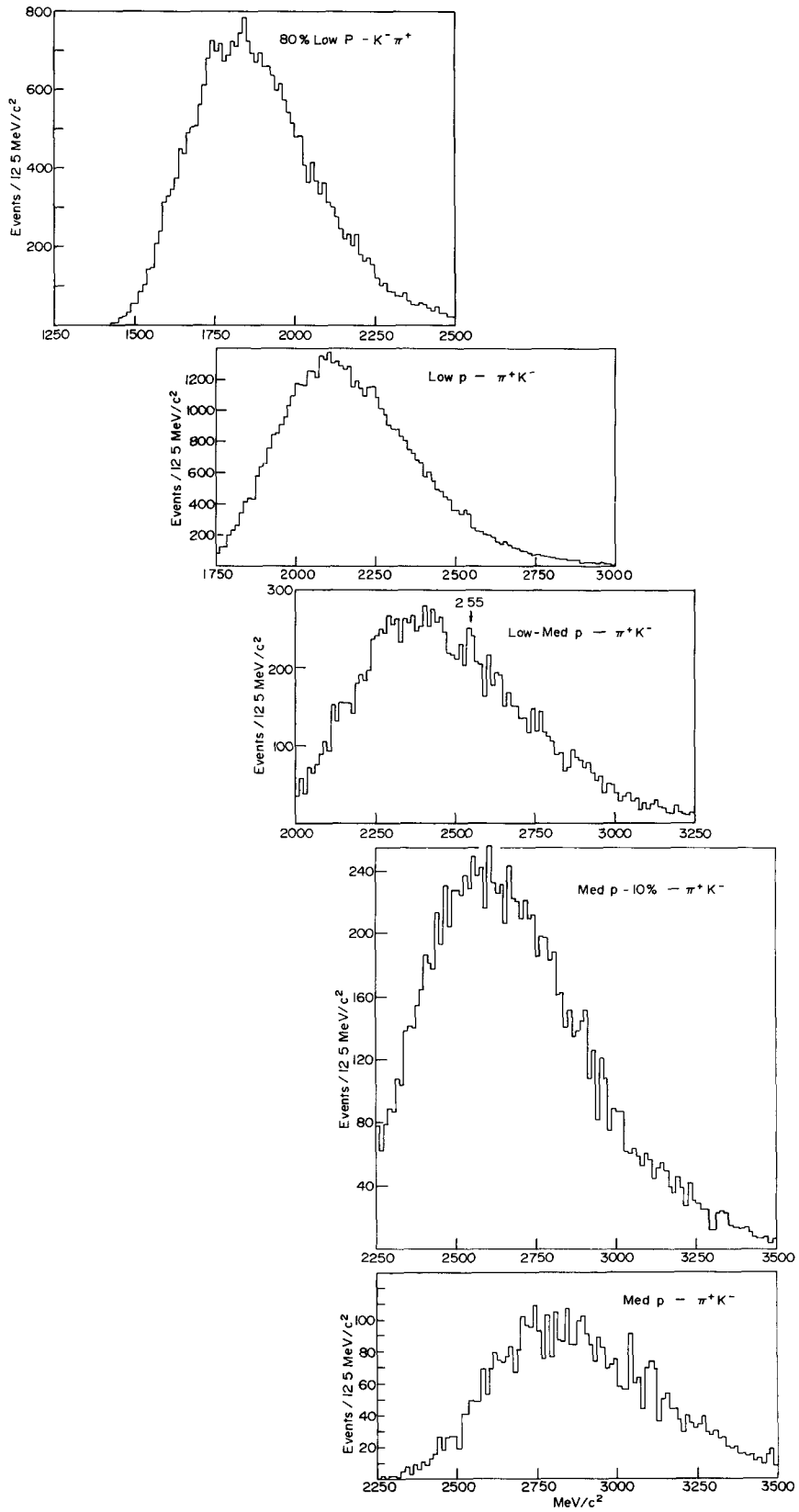


Fig. 26. $K^- \pi^+$ mass spectra for five mass ranges from MIT-BNL.

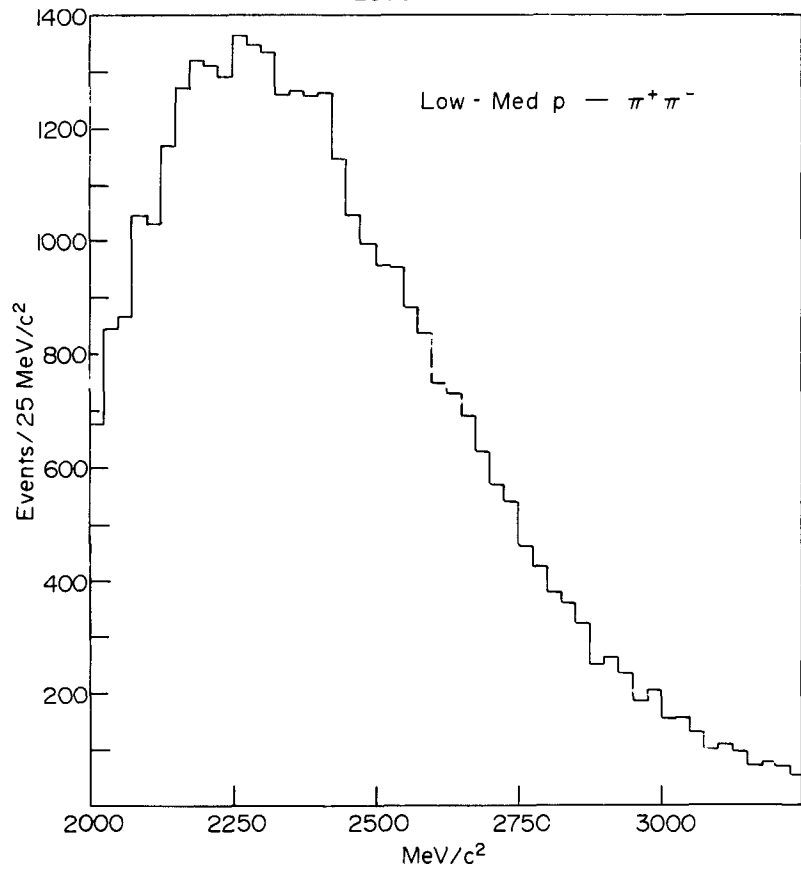
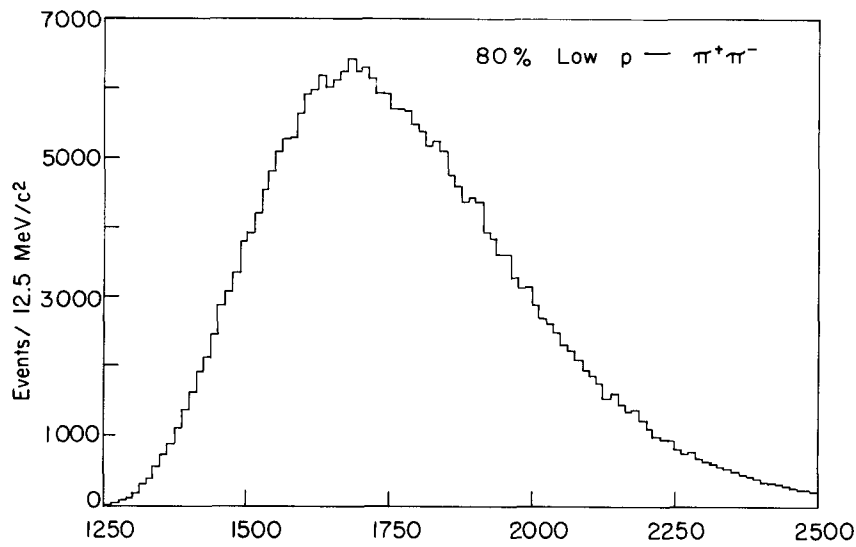


Fig. 27. $\pi^-\pi^+$ mass spectra for two mass ranges from MIT-BNL.

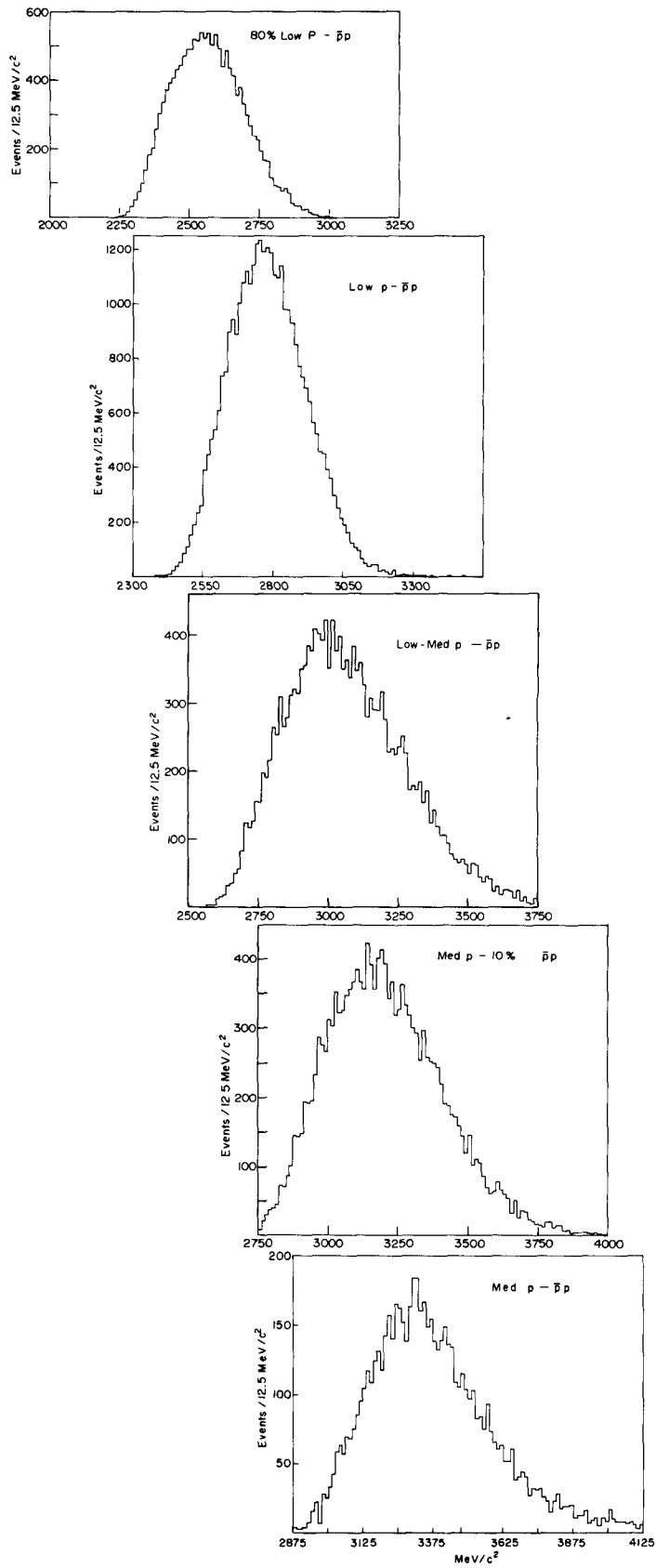


Fig. 28. $\bar{p}p$ mass spectra for five mass ranges from MIT-BNL.

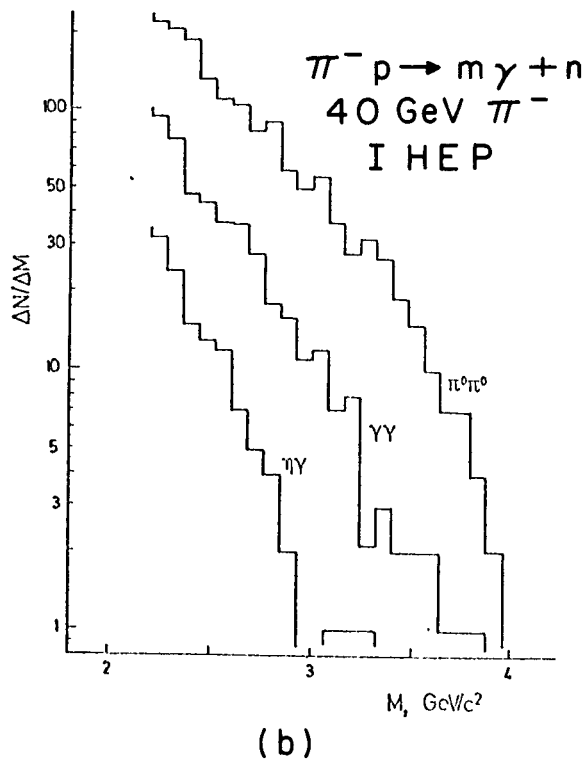
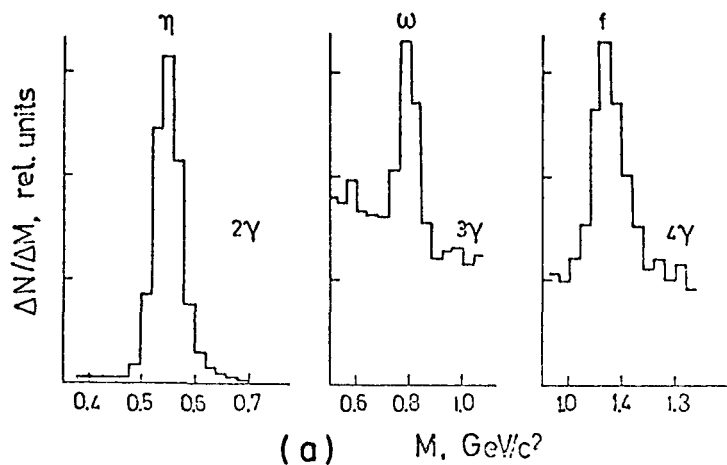


Fig. 29

- a) Invariant mass spectra in the low mass region for the events which fit $\gamma\gamma, \pi^0\gamma$ and $\pi^0\pi^0$ hypotheses. Peaks are seen which correspond to decays $\eta \rightarrow \gamma\gamma, \omega \rightarrow \pi^0\gamma$ and $f \rightarrow \pi^0\pi^0$.
- b) Invariant mass spectra with $M > 2.2 \text{ GeV}$ for the events which fit hypotheses $\pi^0\pi^0, \eta\gamma$ and $\gamma\gamma$.